Monthly Notices
of the
ROYAL ASTRONOMICAL SOCIETY

MNRAS **483,** 2851–2870 (2019)
Advance Access publication 2018 November 30

doi:10.1093/mnras/sty3258

The SAMI Galaxy Survey: observing the environmental quenching of star formation in GAMA groups

A. L. Schaefer,[1,2,3,4] S. M. Croom,[1,3,5] N. Scott,[1,3,5] S. Brough,[3,5,6] J. T. Allen,[1,7] K. Bekki,[8] J. Bland-Hawthorn,[1,5] J. V. Bloom,[1,3] J. J. Bryant,[1,2,3,5] L. Cortese,[8] L. J. M. Davies,[8] C. Federrath,[9] L. M. R. Fogarty,[1] A. W. Green,[7] B. Groves,[5,9] A. M. Hopkins,[7] I. S. Konstantopoulos,[7,10] A. R. López-Sánchez,[7,11] J. S. Lawrence,[7] R. E. McElroy,[12] A. M. Medling,[9,13] M. S. Owers,[11] M. B. Pracy,[1] S. N. Richards,[14] A. S. G. Robotham,[15] J. van de Sande,[1,5] C. Tonini[16] and S. K. Yi[17]

[1]*Sydney Institute for Astronomy, School of Physics, University of Sydney, NSW 2006, Australia*
[2]*Australian Astronomical Optics, AAO-USydney, School of Physics, University of Sydney, NSW 2006, Australia*
[3]*CAASTRO: ARC Centre of Excellence for All-sky Astrophysics*
[4]*Department of Astronomy, University of Wisconsin-Madison, 475 North Charter Street, Madison, WI 53706, USA*
[5]*ARC Centre of Excellence for All-sky Astrophysics in 3 Dimensions (ASTRO 3D)*
[6]*School of Physics, University of New South Wales, NSW 2052, Australia*
[7]*Australian Astronomical Optics, AAO-Macquarie, Faculty of Science and Engineering, Macquarie University, 105 Delhi Rd, North Ryde, NSW 2113, Australia*
[8]*International Centre for Radio Astronomy Research, University of Western Australia, 35 Stirling Highway, Crawley, WA 6009, Australia*
[9]*Research School of Astronomy and Astrophysics, Australian National University, Canberra, ACT 2611, Australia*
[10]*Atlassian, 341 George St Sydney, NSW 2000, Australia*
[11]*Department of Physics and Astronomy, Macquarie University, NSW 2109, Australia*
[12]*Max Planck Institut für Astronomie Königstuhl, 17, 69117, Heidelberg, Germany*
[13]*Ritter Astrophysical Research Center University of Toledo, Toledo, OH 43606, USA*
[14]*SOFIA Science Center, USRA, NASA Ames Research Center, Building N232, M/S 232-12, PO Box 1, Moffett Field, CA 94035-0001, USA*
[15]*SUPA School of Physics, Astronomy, University of St Andrews, St Andrews KY16 9SS, UK*
[16]*School of Physics, University of Melbourne, Parkville 3010, Victoria, Australia*
[17]*Department of Astronomy and Yonsei University Observatory, Yonsei University, Seoul 03722, Republic of Korea*

Accepted 2018 November 27. Received 2018 November 16; in original form 2017 May 5

ABSTRACT

We explore the radial distribution of star formation in galaxies in the SAMI Galaxy Survey as a function of their Local Group environment. Using a sample of galaxies in groups (with halo masses less than $\simeq 10^{14}\,M_\odot$) from the Galaxy And Mass Assembly Survey, we find signatures of environmental quenching in high-mass groups ($M_G > 10^{12.5}\,M_\odot$). The mean integrated specific star formation rate (sSFR) of star-forming galaxies in high-mass groups is lower than for galaxies in low-mass groups or those that are ungrouped, with $\Delta \log(\mathrm{sSFR/yr^{-1}}) = 0.45 \pm 0.07$. This difference is seen at all galaxy stellar masses. In high-mass groups, star-forming galaxies more massive than $M_* \sim 10^{10}\,M_\odot$ have centrally concentrated star formation. These galaxies also lie below the star formation main sequence, which suggests they may be undergoing outside-in quenching. Lower mass galaxies in high-mass groups do not show evidence of concentrated star formation. In groups less massive than $M_G = 10^{12.5}\,M_\odot$, we do not observe these trends. In this regime, we find a modest correlation between centrally concentrated star formation and an enhancement in the total star formation rate, consistent with triggered star formation in these galaxies.

Key words: galaxies: evolution – galaxies: interactions – galaxies: star formation – galaxies: structure – galaxies: groups: general.

⋆ E-mail: aschaefer@astro.wisc.edu

1 INTRODUCTION

Obtaining a physical understanding of the modulation of star formation within galaxies remains an important goal for galaxy evolution studies. Empirically, large galaxy surveys have uncovered broad trends that show star formation depends on both galaxy mass and environment (e.g. Peng et al. 2012). Multiple measurements show that star formation is suppressed in high-density environments (e.g. Lewis et al. 2002), but the detailed physical nature of this suppression is not yet determined.

Processes such as ram pressure stripping or strangulation are thought to play a significant role. Ram pressure stripping occurs when the kinetic interaction between the interstellar medium (ISM) of a galaxy and the intergalactic medium (IGM) forces the gas out of the galaxy (Gunn & Gott 1972). Strangulation, sometimes referred to as starvation, occurs when the infall of gas into the disc of a galaxy is halted, starving the galaxy of fuel for future star formation (Larson, Tinsley & Caldwell 1980). This process can occur when a galaxy falls into a cluster or group and its outer gaseous envelope is heated or removed.

Much of the literature concerning the impact of galaxy environments on star formation has focussed on studies of galaxy clusters. Narrow-band imaging studies of the distribution of Hα emission in the Virgo cluster (e.g. Koopmann & Kenney 2004a,b; Koopmann, Haynes & Catinella 2006) have shown that half of the star-forming galaxies in this cluster have truncated star formation, with the star formation preferentially stopped in the outer parts of discs. This is consistent with the observation of truncated neutral hydrogen gas discs in Virgo (Cayatte et al. 1990). Truncation is also seen in dust (Cortese et al. 2010) and ultraviolet (UV) star formation measurements (Cortese et al. 2012), while there are enhancements seen in central molecular gas (Mok et al. 2017). The degree of truncation depends on the distance from the centre of Virgo (Gavazzi et al. 2013).

The above observations point to ram pressure being the dominant contributor to quenching in clusters such as Virgo, where it is particularly efficient for relatively low-mass galaxies (e.g. Boselli et al. 2014, 2016). Comparing a suite of simulated galaxy orbits with observations of the projected phase-space distribution of galaxies from the SDSS, Oman & Hudson (2016) showed that in high-mass haloes ($>10^{13}$ M$_\odot$) quenching is efficient. However, others suggest lower efficiency (e.g. Wheeler et al. 2014), albeit for galaxies of lower mass.

Although clusters represent the most extreme environments, only $\sim$5 per cent of galaxies exist in rich clusters. Because approximately 40–50 per cent of galaxies exist in groups at $z \sim 0$ (Eke et al. 2004; Robotham et al. 2011), the majority of environment-driven galaxy evolution is likely to occur outside of clusters (e.g. Balogh et al. 2004). Even for cluster galaxies, it is likely that many are quenched prior to infall, via pre-processing in groups (e.g. Zabludoff et al. 1996; Fujita & Goto 2004; Bianconi et al. 2018). Some of this pre-processing may be driven by ram pressure in filaments out to many times the virial radius of a cluster (Bahé et al. 2013). This conclusion is consistent with H I stacking by Brown et al. (2017) that shows a deficit of neutral gas, even in relatively low-mass groups (10^{12}–$10^{13.5}$ M$_\odot$).

Global analysis of star formation in large-scale spectroscopic galaxy surveys (e.g. the Sloan Digital Sky Survey; SDSS) points to environmental quenching being driven by processes that primarily act on satellite galaxies in haloes (e.g. Wetzel, Tinker & Conroy 2012; Wetzel et al. 2013). Satellite quenching may occur with a delay of a few Gyr after infall, followed by quenching on a time-scale of $<$0.8 Gyr. Others have reached the conclusion that the environmental quenching of star formation must be a rapid process (Balogh et al. 2004; Wijesinghe et al. 2011; Brough et al. 2013) based on the scarcity of galaxies in transition between star-forming and passive. However, Rasmussen et al. (2012) find that the integrated star formation rates of star-forming galaxies in groups are suppressed by 40 per cent relative to those of galaxies outside of groups, so they are likely in the process of being quenched. This result is in better agreement with work by von der Linden et al. (2010), who study groups and clusters (typical halo mass of $\sim 10^{14}$ M$_\odot$) and also find star-forming galaxies that are transitioning. The identification of a currently quenching population infers a relatively slow transition (several Gyr). It is plausible that limits in sensitivity and/or aperture effects when using single-fibre spectroscopy have made it difficult to identify galaxies currently in the process of quenching. Taking an alternative approach, Peng, Maiolino & Cochrane (2015) use the difference in stellar metallicity between star-forming and passive galaxies to infer that slower starvation is preferred.

Spatially resolved studies of environmental quenching outside of clusters are considerably more limited. Cibinel et al. (2013) find that the outer parts of disc galaxies are relatively redder in high-mass groups ($>10^{13.5}$ M$_\odot$), compared to those in lower mass groups. Qualitatively similar results are found by the narrow-band Hα Galaxy Group Imaging Survey (HAGGIS; Kulkarni 2015).[1] They find that galaxies below the star formation main sequence in groups typically have compact star formation with a steep radial profile. In contrast, Eigenthaler et al. (2015) find no evidence of the truncation of star formation, as traced by Hα, in Hickson compact groups. These results suggest that radial truncation (presumably driven by ram pressure) is a factor in quenching over at least some range of halo masses in the group regime.

Other authors, using data from single-fibre spectroscopic surveys, have argued that much of the environment-driven evolution of galaxies can be explained by interactions between close pairs. Robotham et al. (2014) showed that galaxies that are both dynamically and spatially close to their nearest neighbour are likely to have disturbed optical morphologies. This idea was expanded upon by Davies et al. (2015), who showed that star formation in galaxies separated by less than $\sim$30 kpc can also be affected. Their data showed that for galaxies in close pairs, the more massive galaxy tended to have its star formation enhanced, while the less massive galaxy had its star formation suppressed. They posited that the tidal disturbance of gas in the more massive galaxy would trigger star formation. While the enhancement of star formation in close pairs was also reported in other studies (e.g. Ellison et al. 2008; Patton et al. 2013), they did not study the suppression of star formation during these interactions. Davies et al. (2016a) showed that galaxies with stellar masses below $\sim 10^{8.5}$ M$_\odot$ become passive only in the presence of a more massive companion and argued that the increasing time-scales for interaction between a galaxy of this mass and a more massive companion are consistent with their star formation being suppressed by strangulation. It is unclear from the research to date whether the environmental suppression of star formation in groups is due to galaxy–galaxy interactions or whether it can be attributed to the impact of the group environment at large.

Taken as a whole, the established literature suggests that in the most massive haloes ram pressure stripping is dominant, and that there is some evidence that ram pressure stripping continues to be

[1] Accessible at: https://edoc.ub.uni-muenchen.de/18818/1/Kulkarni_Sandesh.pdf

important at halo masses in the group regime ($<10^{14}$ M$_\odot$). A valuable route to diagnosing quenching mechanisms is spatially resolved star formation measurements, and this is our focus for the current paper. In previous work (Schaefer et al. 2017), we showed that as the local environment density (defined as fifth nearest neighbour) increases around a galaxy, the specific star formation rate (sSFR; SFR/M$_*$) drops and this reduction in star formation occurs in the outer parts of the galaxy. This infers that in the environments studied quenching occurs from the outside in. In the current paper, we follow on from the results of Schaefer et al. (2017), studying how the spatial distribution of star formation changes in galaxies relative to physically motivated measures of the local environment. In particular, we focus on group properties, the location of galaxies within those groups, and the estimated tidal force acting on each galaxy. Our focus is on galaxies in haloes with mass less than $\sim 10^{14}$ M$_\odot$, as this is where our picture of environmental quenching is currently least clear.

The remainder of this paper has the following layout. In Section 2, we describe our data, discuss our sample selection, and introduce the methods by which we measure the star formation properties of our galaxies. We compare these measurements of the star formation rate distribution to various metrics of the local environment in Section 3, discuss our findings in Section 4, and conclude with Section 5.

We assume a flat lambda cold dark matter cosmology with $H_0 = 70\,\mathrm{km\,s^{-1}\,Mpc^{-1}}$, $\Omega_\mathrm{M} = 0.27$, and $\Omega_\Lambda = 0.73$. Unless otherwise stated, we adopt a Chabrier (2003) stellar initial mass function for calculation of star formation rates.

2 METHODS

2.1 SAMI Data

The data for this study have been taken from the Sydney-Australian Astronomical Observatory Multi-object Integral Field Spectrograph (SAMI; Croom et al. 2012) Galaxy Survey (Bryant et al. 2015) and the Galaxy and Mass Assembly (GAMA; Driver et al. 2011; Hopkins et al. 2013) survey. The SAMI Galaxy Survey is a resolved spectroscopic survey of over 3000 galaxies performed using SAMI, which is mounted on the 3.9 m Anglo-Australian Telescope (AAT) at Siding Spring Observatory in Australia. SAMI comprises 13 optical fibre hexabundles (Bland-Hawthorn et al. 2011; Bryant et al. 2014) plugged into a steel plate at the prime focus of the AAT, 12 of which are used to observe galaxies while the remaining hexabundle observes a standard star. These optical fibres feed into the AAOmega spectrograph, where the light is split into a red arm ($\lambda\lambda$6300–7400 Å) and dispersed at a resolution of $R = 4260$ and a blue arm ($\lambda\lambda$3700–5800 Å) where it is dispersed to a resolution of $R = 1810$ (van de Sande et al. 2017). The SAMI hexabundles are made of 61 optical fibres fused to cover an approximately circular field of view with a 15 arcsec diameter on the sky. Within each hexabundle, the optical fibres fill the aperture with an efficiency of $\sim$73 per cent. As a result, observations of galaxies with SAMI must be dithered to uniformly cover the image. We used approximately 7 pointings of 1800 s integrations for a total 12 600 s exposure. The raw data are reduced using the SAMI data reduction package, which has been written in the PYTHON language[2] and makes use of the 2DFDR pipeline (Croom, Saunders & Heald 2004). The circular fibre cores are resampled on to a regular grid of 50 × 50 0.5 arcsec spaxels. For a full description of the data reduction, see Allen et al. (2015) and for a discussion of representing the fibre data in a regularly gridded data cube see Sharp et al. (2015).

The galaxies observed for the main SAMI Galaxy Survey sample have been drawn from the equatorial regions of the GAMA spectroscopic survey (see Section 2.2). The SAMI survey sample has a stepped selection function in stellar mass with redshift such that the final sample has a nearly uniform distribution of stellar masses. This sample selection covers a wide range of galaxy stellar masses ($10^7 < M_*/\mathrm{M}_\odot < 10^{11.5}$) in the redshift range $0.004 < z < 0.11$ and includes galaxies in a wide variety of environments from non-group galaxies to galaxies in 10^{14} M$_\odot$ group haloes. A thorough discussion of the SAMI target selection is given in Bryant et al. (2015). The SAMI survey augments the main GAMA-selected sample with a targeted sample of $\sim$800 cluster galaxies (Owers et al. 2017), chosen from the 2 Degree Field Galaxy Redshift Survey (Colless et al. 2001) and the Sloan Digital Sky Survey (York et al. 2000; Abazajian et al. 2009). At the time of this analysis, consistent measurements of the stellar masses and local environments surrounding the galaxies in the SAMI cluster sample were not available. This is due to the lack of highly complete spectroscopy and deep, multi-wavelength imaging as is available through the GAMA survey. For this reason, the SAMI cluster galaxies have not been included for this work. There is extensive existing literature on the quenching of star formation in galaxy clusters. However, it is not clear that the processes that act to quench galaxies in clusters will dominate in lower mass haloes. For this reason, we focus on the environmental effects on galaxies in groups. A study comparing the quenching mechanisms operating in clusters and groups will be presented in a future paper.

2.2 GAMA data

GAMA, the parent survey for SAMI, is a deep, highly complete spectroscopic survey of galaxies made in three equatorial regions centred on 9, 12, and 15 h right ascension, with two additional non-equatorial fields that were not used for the SAMI selection. The equatorial fields have 98.5 per cent complete spectroscopy to $r = 19.8$ mag, two magnitudes deeper than the SDSS (Liske et al. 2015).

2.2.1 *Sérsic photometry*

The GAMA survey targeted regions that have been covered by SDSS imaging in the *u*, *g*, *r*, *i*, and *z* photometric bands. These images were reanalysed by Kelvin et al. (2012), who extracted objects from the images and fit single-component Sérsic profiles to galaxies. We have made use of these data products, in particular the measurements of the effective radii (R_e), ellipticities, and position angles extracted from the Sérsic fits to the SDSS *r*-band images.

2.2.2 *Stellar masses*

We have used estimates of the stellar masses of the galaxies in our sample and their companions from version 18 of the GAMA stellar mass catalogue. Stellar masses were computed by Taylor et al. (2011), who used the *ugriz* photometry and local-flow-corrected spectroscopic redshifts (Tonry et al. 2000) to construct the rest-frame spectral energy distribution of each galaxy. These spectral

[2]Astrophysics Source Code Library, ascl.net/1407.006

energy distributions were used to model the stellar mass, star formation history, metallicity, and dust extinction in each galaxy assuming a Chabrier (2003) stellar initial mass function (IMF). These stellar mass estimates are accurate to approximately 0.1 dex for galaxies brighter than $r_{\rm petro} = 19.8$ mag.

2.2.3 *GAMA galaxy group catalogue*

The deep and spectroscopically complete nature of the GAMA survey has allowed the creation of one of the most robust catalogues of galaxy groups made to date. Robotham et al. (2011) used a friends-of-friends linking algorithm to assign galaxies to groups. This two-step process uses both the projected separations of the galaxies and their redshifts to recover the true grouping of galaxies in space. The nature of the algorithm used is such that even pairs of galaxies are identified as groups in the final catalogue. The grouping algorithm locates the central galaxy of a group and computes the group size, multiplicity (number of members above the detection limit), and velocity dispersion. From these measurements, it is possible to derive a number of properties of the group and its members, including the total dynamical mass of the halo, the projected distance of each galaxy from the centre of the group, and the line-of-sight velocity of each galaxy with respect to the group centre. For an in-depth discussion of the group-finding algorithm used to derive the catalogue, see Robotham et al. (2011), though note that at the time the original paper was published, the GAMA survey was still ongoing and consequently the size of the group catalogue and the spectroscopic completeness have since increased. We use the GAMA Galaxy Group Catalogue version 9. The group halo masses and the associated uncertainties were calibrated by applying the group-finding algorithm to a set of mock catalogues from the Millennium Simulation (Springel et al. 2005). The uncertainty in group mass was found to be a function of the number of galaxies in each group ($N_{\rm fof}$), $\log(M_{\rm err}/{\rm M}_\odot) = 1.0 - 0.43\log(N_{\rm fof})$. This relation gives group mass errors of $\sim$0.87 dex for the lowest mass groups and $\sim$0.3 dex for the most massive groups in our sample. A follow-up study of the GAMA group catalogue using weak gravitational lensing demonstrated that the estimated group masses are unbiased down to at least $M_{\rm G} = 10^{13}\,{\rm M}_\odot$ (Viola et al. 2015).

2.3 Sample selection

We have selected galaxies from the SAMI Galaxy Survey in the GAMA regions. At the time of writing, there are 1295 galaxies from the SAMI main survey that have been observed and for which the data have been reduced. These galaxies comprise the SAMI internal data release v0.9.1. Our study of the spatially resolved star formation properties of galaxies requires the selection of star-forming galaxies. Our method for selecting our star-forming sample mimics that of Schaefer et al. (2017).

To measure whether a galaxy has any ongoing star formation, we have integrated the data cubes across both spatial axes and from the resulting spectrum we measure the equivalent width of the Hα emission (EW$_{\rm H\alpha}$), correcting for the underlying stellar absorption. If the absolute value of EW$_{\rm H\alpha}$ is less than 1 Å, we say that the galaxy is passive. This Hα equivalent width cutoff corresponds to an sSFR limit of approximately 10^{-12} yr^{-1} and eliminates 253 non-star-forming galaxies from our sample. In addition to this constraint, we classify galaxies based on their emission-line ratios in the central 2 arcsec. Based on the ratios of [N II] λ6583 to Hα and [O III] λ5007 to Hβ in this inner spectrum, we classify galaxies as either star-forming, composite, or active galactic nucleus (AGN)/low-ionization nuclear emission-line region (LINER) based on their location on the Baldwin, Phillips & Terlevich (BPT; 1981) diagram. Galaxies with line ratios that place them above both the Kewley et al. (2001) and Kauffmann et al. (2003b) lines are classified as AGN/LINER, of which we find 333 in our sample. Between these two constraints are a total of 165 composite objects and below both lines are the star-forming objects. Below we will refer to central spectra that are above the Kauffmann et al. (2003b) line as AGN-like, noting that the emission is not necessarily due to accretion on to a supermassive black hole.

Recent advances have been made in decomposing the emission lines in galaxies hosting AGNs into star-forming and AGN-excited components. Davies et al. (2016) proposed a technique whereby the lines are modelled as a linear combination of spectra from the uncontaminated AGN and H II regions within a given galaxy. Due to the redshift of the galaxies in our sample, this technique cannot be applied. The physical resolution of SAMI is typically $\sim$1 kpc, meaning that a pure AGN basis spectrum cannot reliably be extracted from the data.

To reduce the effect of having hexabundles with a finite aperture on measuring the spatial distribution of star formation, we also limit the sizes of the galaxies that we include in our analysis. Twenty-six galaxies with effective radii greater than 15 arcsec are rejected, as are 149 galaxies for which the seeing of the observation is greater than $1R_{\rm e}$. We also excluded galaxies that have ellipticity values greater than 0.7 to eliminate 200 edge-on systems. Note that some galaxies have been rejected based on more than one constraint.

Our final star-forming sample comprises 325 galaxies, including 158 galaxies not assigned to groups and 167 galaxies in groups. From here onwards, we will refer to this sample as the final star-forming sample (or Final-SF). We will refer to the sample of galaxies that meet all other cuts but that have EW$_{\rm H\alpha} < 1$Å as our passive sample (Final-Pas). We show the distribution of halo masses for our final star-forming sample in Fig. 1, which covers a range of masses between 10^9 and $10^{14.5}$ M$_\odot$. These histograms do not include galaxies that have not been identified as belonging to a group in the GAMA Galaxy Group Catalogue.

Throughout this paper, we utilize several different subsamples, using the selections described above. These allow us to test the robustness of our conclusions to changes in our selection criteria. These are summarized in Table 1. The full samples (Full-Em and Full-Pas for those above and below the EW$_{\rm H\alpha} = 1$ Å limit, respectively) contain almost all galaxies, only removing a very small fraction with $R_{\rm e} > 15$ arcsec. The Inc-Em and Inc-Pas samples also have the inclination and size cuts applied (but not any rejection of central AGN-like emission). The Final-SF and Final-Pas samples also apply the constraint removing objects with central AGN-like spectra.

2.3.1 *Possible effects of excluding AGN-like galaxies*

The sample selection criteria introduced in Section 2.3 were devised to provide a sample of galaxies where our measurements of the spatial distribution of star formation are robust. As a result, the Final-SF sample is a relatively small fraction of the entire sample. Some galaxies that have been removed from our sample failed to satisfy multiple criteria for selection. In particular, of the 333 galaxies that were identified as having AGN-like emission in their centres, 203 simultaneously failed our integrated EW$_{\rm H\alpha}$ cut. Given the number of galaxies not included, it is important

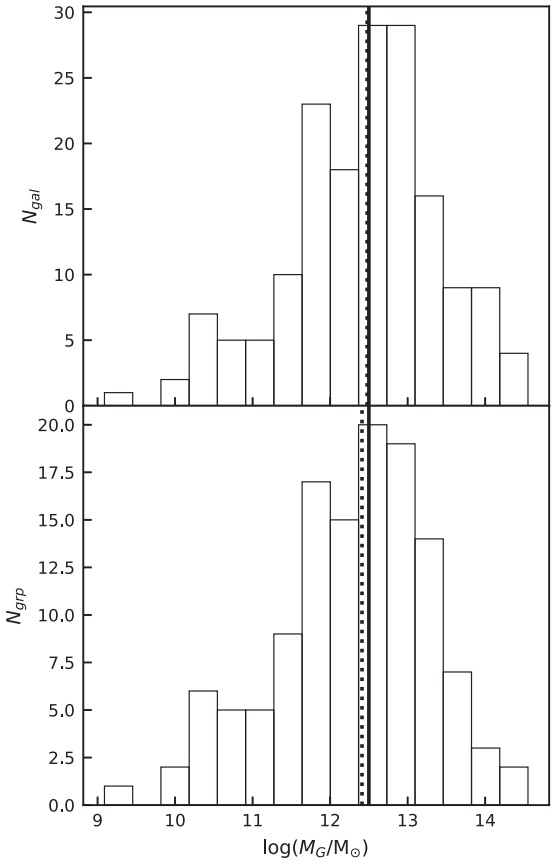

Figure 1. The distribution of halo masses for galaxies detected as being members of groups in our final star-forming sample. In the upper histogram, we show the number of galaxies in each interval of group mass, while in the lower histogram we show the number of individual groups in each interval of group mass. The vertical black solid line marks the $10^{12.5}$ M$_\odot$ division used throughout this work. The dotted line shows the median group mass, $M_G = 10^{12.46}$ M$_\odot$.

to understand whether our cuts have biased the final star-forming sample.

Galaxies with EW$_{H\alpha} > 1$ Å tend to have high stellar masses and preferentially occupy dense environments. As was noted above, of the 253 galaxies that did not satisfy our EW$_{H\alpha}$ criterion, 203 have central emission-line ratios that classify them as AGN-like. This is largely because quenched galaxies often have weak LINER-like emission. Nevertheless, it is possible that we are preferentially excluding galaxies in dense environments based on their central emission-line ratios that would otherwise have detectable star formation. We test for this possibility using a logistic regression (Cox 1958; Walker & Duncan 1967) that models the probability of a galaxy having central AGN-like emission-line ratios as a function of log (M_*/M$_\odot$) and fifth-nearest-neighbour environment surface density log (Σ_5/Mpc^2) as measured by the GAMA survey (Brough et al. 2013). We use Σ_5 to quantify the environment in this context because it provides a measure of the environment density of galaxies that can be measured for our entire sample, including galaxies not found in groups. Within our group sample, Σ_5 is correlated with the group mass, and other metrics of environment density. While the following test utilizes Σ_5 as a probe of environment, the result is therefore applicable to other measures of environment (in fact the same result is found if we use group mass rather than Σ_5 for only the group galaxies).

Our test uses the 477 galaxies in the Inc-Em sample (see Table 1). These have integrated EW$_{H\alpha}$ larger than 1 Å and satisfy all of the data quality constraints imposed on our sample [point spread function (PSF) full width at half-maximum (FWHM)/$R_r < 0.75$, ellipticity < 0.7, $R_e < 15$ arcsec, and the environment density flag in the GAMA catalogue is set to 0] and include galaxies with AGN-like central spectra. The distribution of these galaxies can be seen in Fig. 2. A clear division between the objects with central AGN-like spectra (red points) and those that are star-forming (blue points) can be seen. This division is a strong function of stellar mass, but there is no visible separation by environment. The results of the logistic regression confirm this and can be found in Table 2. This analysis finds that within our sample the probability of a galaxy hosting AGN-like central emission-line ratios is strongly correlated with its stellar mass (correlation coefficient 3.50 ± 0.35), but that there is no significant relationship with Σ_5 (correlation coefficient 0.25 ± 0.22).[3] Thus, our removal of AGNs (in order to measure robust star formation morphologies) does not introduce a bias that depends on the environment. It does introduce a bias as a function of stellar mass. To negate this we will, where possible, compare results as a function of mass. While largely focusing on the Final-SF sample only for the remainder of this paper, we will discuss the impact of leaving central AGN-like galaxies in the sample at various points.

2.3.2 *The distribution of galaxy apparent sizes as a function of stellar mass*

The selection of our Final-SF sample included the criterion that the PSF FWHM for an observation must not exceed 0.75 times the *r*-band effective radius of the galaxy. This constraint was imposed to ensure that the measurement of the spatial extent of star formation is as robust to PSF effects as possible. However, the possibility exists that this criterion may adversely affect our coverage of low-mass galaxies. Splitting the full sample into three evenly spaced bins of stellar mass (log (M_*/M$_\odot$) < 9.1, $9.1 \leq$ log (M_*/M$_\odot$) < 10.1, and log (M_*/M$_\odot$) ≥ 10.1), we compare the means of the *r*-band effective radii in these ranges. These values are 4.65 ± 0.38, 5.03 ± 0.35, and 4.16 ± 0.47 arcsec for the low-, intermediate-, and high-stellar-mass bins, respectively. These are broadly consistent with each other thanks to the selection of the main SAMI Galaxy Survey that has a stepped selection function in stellar mass and redshift. The conclusion that we draw from this is that the removal of galaxies that are small relative to the PSF will not strongly affect low-mass galaxies any more than high-mass galaxies, and consequently any trends inferred to be a function of stellar mass are not impacted by this selection criterion.

2.3.3 *Comparison between different group environments*

Interpreting any variation in the star-forming properties of galaxies between different subsamples requires that there be no major discrepancies in the galaxy properties between the different subsamples. In Section 3, we introduce three subsamples: (i) galaxies that are not in groups, (ii) galaxies that are in the Robotham et al.

[3]These coefficients can be interpreted as the increase in the log odds, ln (p/(1 − p)), of a galaxy hosting central AGN/LINER/composite emission-line ratios per unit increase in log(M_*/M$_\odot$) or log(Σ_5/Mpc^2).

Table 1. A description of the various samples used throughout this work, and the number of objects in each. The Inc-Pas and Final-Pas samples are the same since the identification of AGN-like emission becomes uncertain in galaxies with weak emission lines.

Name	Abbreviation	Description	Number
Full Emission line	Full-Em	All galaxies with $EW_{H\alpha} > 1$ Å and $R_e < 15$ arcsec	1012
Full Passive	Full-Pas	All galaxies with $EW_{H\alpha} \leq 1$ Å and $R_e < 15$ arcsec	246
Inc. Emission line	Inc-Em	All galaxies with $EW_{H\alpha} > 1$ Å and $R_e < 15$ arcsec, ellipticity < 0.7, seeing/$R_e < 0.75$, seeing $<$ 4 arcsec, includes AGN-like central spectra	477
Inc. passive	Inc-Pas	All galaxies with $EW_{H\alpha} \leq 1$ Å and $R_e < 15$ arcsec, ellipticity < 0.7, seeing/$R_e < 0.75$, seeing $<$ 4 arcsec	118
Final star-forming	Final-SF	All galaxies with $EW_{H\alpha} > 1$ Å and $R_e < 15$ arcsec, ellipticity < 0.7, seeing/$R_e < 0.75$, seeing $<$ 4 arcsec, excluding AGN-like central spectra	325
Final passive	Final-Pas	All galaxies with $EW_{H\alpha} \leq 1$ Å and $R_e < 15$ arcsec, ellipticity < 0.7, seeing/$R_e < 0.75$, seeing $<$ 4 arcsec	118

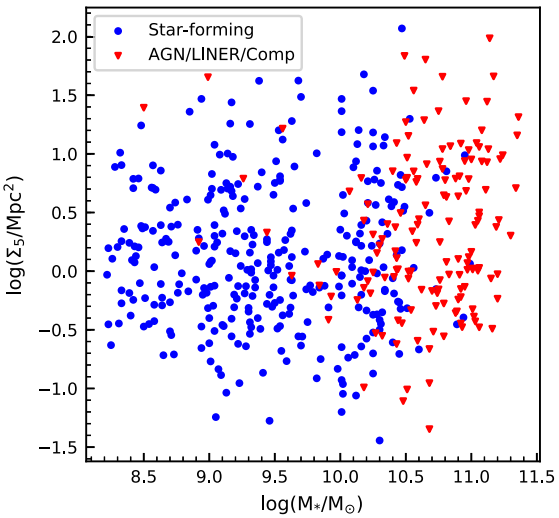

Figure 2. The distribution of stellar mass versus fifth-nearest-neighbour density for galaxies that are selected in our star-forming sample (blue circles) and those that have been rejected due to central AGN-like emission (red triangles). The separation between star formation and AGN-like emission is only dependent on stellar mass.

Table 2. The results of a logistic regression to determine the probability of a galaxy having a central AGN-like spectrum as a function of stellar mass and environment density. Column (1) shows the regression coefficients that represent the change in the log odds of a galaxy hosting a central AGN-like spectrum. Column (2) is the standard error on the coefficients, column (3) is the ratio of the standard error to the coefficient, and column (4) is the p-value against the null hypothesis. The probability of a galaxy hosting central AGN-like emission is correlated with stellar mass, but not significantly with environment.

	Coeff. (1)	Standard error (2)	z-value (3)	$P(z=0)$ (4)
Intercept	−36.5	3.6	−10.1	4.3×10^{-24}
$\log(M_*/M_\odot)$	3.50	0.35	10.1	8.0×10^{-24}
$\log(\Sigma_5/\mathrm{Mpc}^2)$	0.25	0.22	1.16	0.25

(2011) group catalogue with halo masses below $10^{12.5}$ $M_\odot$, and (iii) galaxies in groups with halo masses greater than $10^{12.5}$ $M_\odot$. Fig. 1 shows the distribution of group halo masses. The mean halo masses for the samples above and below our $10^{12.5}$ $M_\odot$ threshold are $10^{13.2}$ and $10^{11.7}$ $M_\odot$, respectively. It should be noted that there are only a handful of galaxies included that exist in haloes of mass greater than 10^{14} $M_\odot$. Therefore, our results reflect the role of group rather than cluster environments (where the nominal dividing line between the two is typically taken to be 10^{14} $M_\odot$).

For the star-forming galaxies that satisfy the selection criteria outlined above, a Kolmogorov–Smirnov (K–S) test indicates no statistically significant differences in the distributions of stellar mass, effective radius, or redshift between the three environment samples ($D_{KS} < 0.2$ and $p > 0.3$ between each variable in each group mass bin). However, given that errors in group mass can be large for low-mass haloes we expect some overlap in halo mass between the ungrouped and low-mass-group samples. We compare the environments in these two samples using the nth nearest neighbour density [with the velocity limit of 1000 km s^{-1} and the same density defining sample as used by Schaefer et al. (2017)]. These surface density measurements are described in full by Brough et al. (2013). Using a K–S test, the nth-nearest-neighbour density is found to be significantly different between the ungrouped and low-mass-group samples for all n values tested: $n = 5$ (Σ_5; $D_{KS} = 0.20$, $p = 0.02$), $n = 3$ (Σ_3; $D_{KS} = 0.26$, $p = 0.0005$) and $n = 1$ (Σ_1; $D_{KS} = 0.533$, $p = 10^{-14}$). The increased significance for smaller n suggests that the low-mass group is dominated by groups of low multiplicity, including pairs.

Given that the mass, redshift, and size distribution of our galaxies is the same for all samples, and that the GAMA spectroscopic completeness is over 98 per cent, it is clear that although there will be some overlap in halo mass between the ungrouped and low-mass-group samples, on average they correspond to different environments.

2.4 Analysis of SAMI data

The analysis of the SAMI data is as described in Schaefer et al. (2017), but for completeness we summarize the process here.

2.4.1 Annular Voronoi binning

To facilitate a robust correction for dust attenuation along the line of sight, we applied annular Voronoi binning to the SAMI data cubes. Spaxels are added together in elliptical annuli to a signal-to-noise ratio of 10 Å^{-1} in the continuum at the wavelength of the Hβ line. An adaptive binning scheme has the advantage of providing sufficient signal to allow the subtraction of the Hβ absorption line and thus an accurate correction for dust extinction. This binning additionally ensures that the spatial scale over which a single dust correction is applied is minimized, while further ensuring that the radial structure in each galaxy is preserved. We

have binned the SAMI data in 0.5-arcsec-wide elliptical annuli that are defined by the ellipticity and position angle obtained from the GAMA Sérsic photometry. This technique is outlined in Schaefer et al. (2017).

2.4.2 *Spectral fitting with* LZIFU

We fitted the spectrum within each annular Voronoi bin using LZIFU (Ho et al. 2016). LZIFU is a spectral fitting pipeline written in the Interactive Data Language (IDL). It utilizes the Penalised Pixel Fitting algorithm (PPXF; Cappellari & Emsellem 2004) to model the stellar continuum light from each galaxy. For each spectrum we fitted a linear combination of simple stellar population models from the MILES library (Vazdekis et al. 2010) with an 8th degree multiplicative polynomial to take into account any residual flux calibration errors and the reddening of the continuum from astrophysical sources. We used a 65-template subset of the full MILES library. This subset covers 5 metallicities from $[Z/H] = -1.71$ to 0.22 and 13 ages spaced logarithmically in the range 0.063–14 Gyr. The continuum model derived by PPXF was subtracted from the data, and the emission lines, including Hα and Hβ, were fitted with single-component Gaussians using the MPFIT routine (Markwardt 2009).

2.5 Star-forming properties of galaxies

We use a number of metrics to determine the impact of the group environment on the star formation in the galaxies in our sample.

2.5.1 *Integrated star formation rates*

We calculated the total star formation rate within the SAMI aperture by adding the dust-corrected flux from each annular Voronoi bin. Dust extinction corrections are applied by measuring the departure of the Balmer decrement, the ratio of the measured Hα flux to Hβ flux (BD; $f_{\mathrm{H}\alpha}/f_{\mathrm{H}\beta}$), from the canonical value of 2.86 predicted for Case B recombination under standard conditions. Under the assumption that the intervening dust forms a foreground screen to the H II regions in our target galaxies (Calzetti 2001) and using the Cardelli, Clayton & Mathis (1989) dust extinction curve, the obscuration-corrected Hα flux is

$$F_{\mathrm{H}\alpha} = f_{\mathrm{H}\alpha}\left(\frac{\mathrm{BD}}{2.86}\right)^{2.36} \quad (1)$$

in each spectrum. In cases where the signal-to-noise ratio for the Hβ emission line is less than 3, or the measured Balmer decrement is less than 2.86, we assume no dust extinction and use the raw Hα flux. Spaxels with emission lines not produced by star formation, as determined by their location on the BPT diagram, are rejected. Integrating the dust-corrected fluxes over the SAMI aperture gives the integrated flux, which is converted to a luminosity using the redshift of each galaxy

$$L(\mathrm{H}\alpha) = 4\pi d_L^2\, F(\mathrm{H}\alpha), \quad (2)$$

where d_L is the luminosity distance to the galaxy. We calculate the star formation rates in our galaxies with the Kennicutt (1998) relation assuming a Chabrier (2003) IMF:

$$\mathrm{SFR} = \frac{L_{\mathrm{H}\alpha}\,(W)}{2.16\times10^{34}}\,\mathrm{M}_\odot\,\mathrm{yr}^{-1}. \quad (3)$$

The estimated uncertainty on these star formation rates consists of several components. The random errors from fluxes in each annular Voronoi bin are combined and contribute an average uncertainty of 0.015 dex to the star formation rate measurements. The dominant component of our error budget comes from uncertainties in the calibration of equation (3). Kewley et al. (2002) measured a scatter of 10 per cent between the Hα and infrared star formation rates for an error contribution of 0.05 dex. Combining these uncertainties with those of the stellar masses gives specific star formation rate errors that average 0.12 dex.

2.5.2 *The spatial distribution of star formation*

We quantify the radial extent of star formation in galaxies within our sample by making use of the ratio $r_{50,\mathrm{H}\alpha}/r_{50,\mathrm{cont}}$, described in Schaefer et al. (2017). This measurement compares the radius within which half of the dust-corrected Hα emission emanates to the radius containing half of the continuum light from the part of the galaxy that lies within the view of the SAMI hexabundles. These radii are calculated by measuring the curve-of-growth for the emission or continuum light. In calculating the curves-of-growth, we have made the assumption that galaxies in our sample are idealized thin discs and any ellipticity is due to their inclination to our line of sight. The ellipticity and position angle on the sky are taken from the GAMA Sèrsic photometric fits to SDSS *r*-band images. An in-depth discussion of the measurement, advantages of, and systematic effects that can arise by making this measurement on galaxies observed with 15 arcsec integral field units can be found in Schaefer et al. (2017).

We estimate the uncertainty on this quantity using a Monte Carlo approach. The measured values of the Hα and Hβ fluxes, and the estimated galaxy ellipticities and position angles, were shifted by a random amount corresponding to the measurement errors on each quantity. The error distributions were assumed to be Gaussian. This process was repeated 1000 times for each galaxy, and $r_{50,\mathrm{H}\alpha}/r_{50,\mathrm{cont}}$ was remeasured. The error on this quantity is calculated as the standard deviation of the resulting distribution of measured values. For the galaxies in our final star-forming sample, this typically results in an error of 0.02 on $r_{50,\mathrm{H}\alpha}/r_{50,\mathrm{cont}}$, the majority of which is accounted for by the errors on the ellipticity and position angle of the galaxy.

Another source of potential uncertainty is the effect of the seeing on our measurement of the spatial extent of star formation. The impact of the seeing is to convolve the Hα and continuum images of the galaxy with the PSF. If the ratio $r_{50,\mathrm{H}\alpha}/r_{50,\mathrm{cont}}$ is intrinsically close to 1, then convolution with the PSF will not lead to a large change in the observed ratio. This is because the numerator and denominator of the fraction will change by roughly the same amount. If Hα is more extended than the continuum, the fractional increase in $r_{50,\mathrm{H}\alpha}$ will be smaller than for $r_{50,\mathrm{cont}}$ after the convolution. If Hα is less extended than the continuum, then the fractional increase in $r_{50,\mathrm{H}\alpha}$ will be larger than for $r_{50,\mathrm{cont}}$. Thus, the effect of the seeing is to force the observed value of $r_{50,\mathrm{H}\alpha}/r_{50,\mathrm{cont}}$ towards 1.

Using a suite of toy model galaxies, in which we simulated the Hα and continuum light as simple Gaussian distributions with varying sizes, we investigated the magnitude of this bias. The images of these model galaxies were convolved with a 2.5 arcsec Gaussian PSF. When the input $\log(r_{50,\mathrm{H}\alpha}/r_{50,\mathrm{cont}})$ was between -0.2 and 0.2, the seeing changed the measured value by 0.04 on average after convolution. For galaxies with very centrally concentrated star formation, this systematic can be larger, depending on the intrinsic

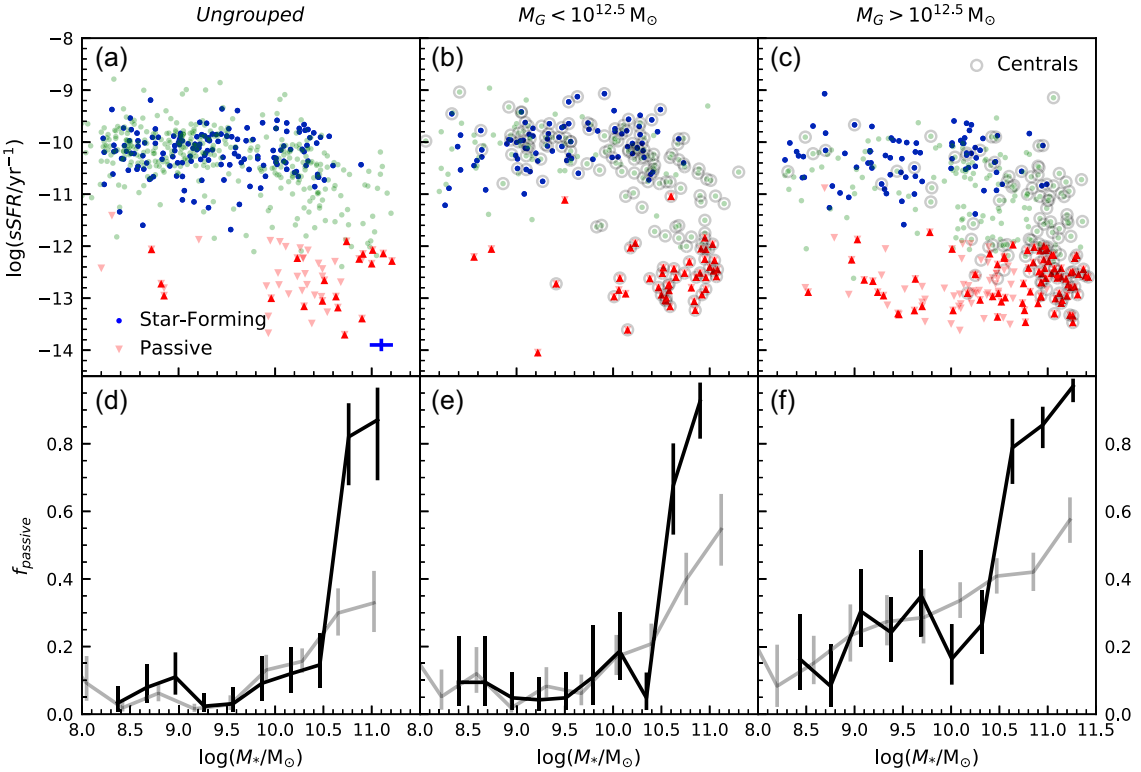

Figure 3. The top row (panels *a–c*) shows the sSFR of star-forming galaxies in our final star-forming sample (blue points) and final passive sample (red triangles) as a function of stellar mass, $\log(M_*/M_\odot)$, in ungrouped galaxies (left), groups with halo mass less than $10^{12.5}\,M_\odot$ (centre), and groups more massive than $10^{12.5}\,M_\odot$ (right). Markers surrounded by grey circles represent galaxies that are the centrals of their halo. In addition to galaxies in the Final-SF sample, we also show the sSFR estimates for the Full-SF and Full-Pas galaxies in light green and light red, respectively. The typical error on the stellar mass and star formation rates for star-forming galaxies are shown at the lower right of panel *a*. The lower row (panels *d–f*) shows the fraction of galaxies that were classified as passive in bins of stellar mass for galaxies satisfying our final selection criteria (black) and the full SAMI sample (grey).

size of the Hα distribution. The effect of the seeing is therefore to reduce the scatter in the measured value of $r_{50,H\alpha}/r_{50,cont}$. While the slope of any trends may be affected slightly, we will make use of Spearman rank correlation tests where appropriate, as this statistic is less sensitive to the change in slope of a correlation in this situation.

As explained in Schaefer et al. (2017), the largest source of uncertainty is the amount of star formation outside of the SAMI aperture. There is no systematic difference in the radial coverage of galaxies between environments in our sample.

3 RESULTS

3.1 Group mass and integrated star formation rates

There is a significant body of work in the literature that focuses on how the star formation rates of galaxies and the fraction of passive galaxies change with stellar mass and environment density (e.g. Peng et al. 2010; Wijesinghe et al. 2011, 2012; Peng et al. 2012; Wetzel et al. 2012; Alpaslan et al. 2015; Davies et al. 2016a). These results are generally based on large-scale single-fibre spectroscopic or photometric surveys. With a representative sample of 325 star-forming galaxies, our primary aim in this paper is not to duplicate previous results from single-fibre surveys but to use the spatially resolved star formation measurements from SAMI to investigate how the location of star formation is modulated by the environment. However, in this section we will briefly discuss our integrated star formation rates and examine whether there are any trends with the environment.

We quantify the effect of group environments on the star-forming properties of galaxies by comparing the sSFRs of galaxies to the masses of their parent group haloes. In Fig. 3, we split our entire sample into three intervals of halo mass. A non-grouped sample, which comprises galaxies that do not appear in the GAMA Galaxy Group Catalogue (Robotham et al. 2011), a low-mass group sample with groups that have multiple galaxies within haloes of mass below $10^{12.5}\,M_\odot$, and a high-mass group sample with galaxies in group haloes more massive than $10^{12.5}\,M_\odot$. This boundary was chosen to approximately evenly split the grouped galaxy sample in two, and corresponds approximately to the threshold mass at which environmental effects are seen in other surveys (e.g. Rudnick et al. 2017). The mean halo mass in each subsample is $10^{13.2}\,M_\odot$ for galaxies in the high-mass groups and $10^{11.7}\,M_\odot$ for galaxies in the low-mass groups. We note that group masses here are derived from the dynamics of galaxies within each halo. For galaxies in the ungrouped subsample, the method of Robotham et al. (2011) is unable to estimate the halo mass. Based on the tight correlation between total stellar mass within a group and its halo mass presented by Yang et al. (2007), we estimate that the most massive haloes in the ungrouped sample will be of order $10^{11} - 10^{12}\,M_\odot$ but are unlikely to host many satellite galaxies brighter than the GAMA detection limit. We will not use this kind of estimate for the remainder of this paper.

In the upper row of panels of Fig. 3, we show the sSFRs

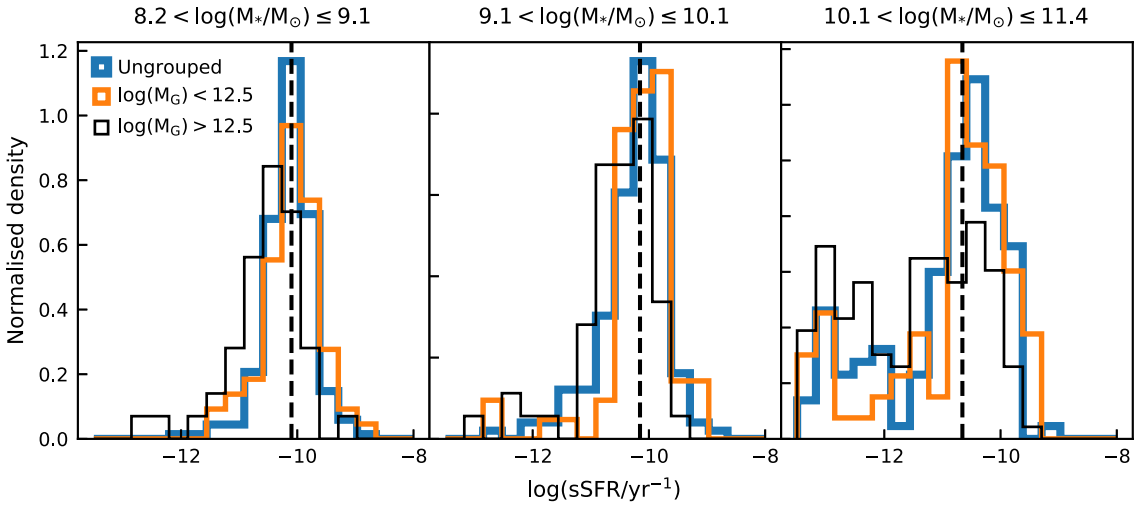

Figure 4. The normalized distribution of sSFRs for ungrouped galaxies (blue), galaxies in groups with $M_G < 10^{12.5}\,M_\odot$ (orange) and galaxies in groups with $M_G > 10^{12.5}\,M_\odot$ (black). We show this separately for three different intervals of galaxy stellar mass. This includes galaxies that have central AGN-like emission (using the Full-Em sample), but only star-forming spaxels are included in the estimation of the sSFR. The vertical black dashed line represents the median sSFR for the ungrouped galaxies in each stellar mass interval. In all three stellar mass intervals, galaxies in the higher mass groups have a systematically lower sSFR.

of our star-forming sample using blue circles and of our passive galaxy sample with red triangles. Objects that are not in the final samples (Final-SF or Final-Pas) are shown as green (for $EW_{H\alpha} > 1$Å) and light red (for $EW_{H\alpha} < 1$ Å); these include galaxies that have been removed due to central AGN-like emission or due to size/inclination cuts. At low stellar mass (below $\sim 10^{10}\,M_\odot$) the distribution of the sSFR is the same for both our star-forming sample and the galaxies rejected. However, at higher stellar mass, galaxies that have been rejected are preferentially at a lower sSFR. This is because of the increasing contribution from objects with central AGN-like emission as stellar mass increases.

In all environments, there is an increase in the passive fraction of galaxies that satisfy our selection criteria at a stellar mass of approximately $10^{10.5}\,M_\odot$, in agreement with numerous previous studies (e.g. Kauffmann et al. 2003a; Geha et al. 2012). The passive fraction based on galaxies that satisfy our final selection criteria is shown by the solid black lines in the lower panels of Fig. 3. We note that if all galaxies in the SAMI sample are included, the rise in passive fraction with stellar mass is more gradual (grey lines). This more gradual trend is consistent with the results presented by Wetzel et al. (2012), and is driven by objects that are rejected on the basis of having central AGN-like emission. Overall, our passive fraction for the entire sample is somewhat lower than Wetzel et al.'s (2012). The cause of this discrepancy is likely to be because Wetzel et al. (2012) define a galaxy as passive if its specific star formation rate is below $10^{-11}\,yr^{-1}$, while our integrated Hα equivalent width limit corresponds to an sSFR of approximately a factor of 10 lower.

When using the full sample (Full-Em and Full-Pas) we find a difference in the passive fraction of low-mass galaxies (below $10^{10.5}\,M_\odot$). The passive fraction is 7 ± 1 per cent, 7 ± 1 per cent, and 29 ± 3 per cent for the ungrouped, low-group-mass, and high-group-mass samples, respectively. While calculating the passive fraction of galaxies is not the main focus of this work, our results are qualitatively consistent with results found in the literature.

In addition to the increased passive fraction of galaxies in the most massive groups, the sSFRs of star-forming galaxies are reduced in dense environments. This is shown by the sSFR distributions in Fig. 4, measured in three independent stellar mass intervals (chosen to have an approximately equal number of galaxies from our final star-forming sample). Here we use all galaxies with $EW_{H\alpha} > 1$ Å (i.e. the Full-EM sample, which includes all blue and green points in Fig. 3) as we are just concerned with integrated values, not with whether we can resolve structure. The mean sSFRs for each environment and stellar mass interval are listed in Table 3. In every stellar mass interval, we see a significant decrease in the mean sSFR in the highest mass groups, with the difference between the ungrouped and high-mass groups being $\Delta\log(\mathrm{sSFR/yr^{-1}}) = -0.38 \pm 0.10$, -0.41 ± 0.13, and -0.64 ± 0.14 for the stellar mass intervals $M_* < 10^{9.1}\,M_\odot$, $10^{9.1} < M_* < 10^{10.1}\,M_\odot$, and $M_* > 10^{10.1}\,M_\odot$, respectively. If we use all spaxels (including AGN–like spaxels), we find the same differential trends (although the sSFR can be biased high by the non-SF contribution, we find the same bias in different environments, leading to the same differential between environments). Likewise, we find the same result if we restrict our sample to just our Final-SF sample (blue points in Fig. 3), although the smaller number of galaxies results in larger uncertainties.

Fig. 4 shows that the sSFR distribution changes in two ways as group mass increases. First, there is a shift of the peak sSFR. This is particularly noticeable at low/intermediate stellar mass. Secondly, there are an increasing number of galaxies in the low-sSFR tail as we move to higher mass groups. The exact number of galaxies in the low-sSFR tail will depend on the threshold used to define the star-forming sample and this will influence the measured mean sSFR. However, given that we are using the full galaxy sample and that we have shown earlier that there are no environmentally dependent biases in the sample selection, this shows that star-forming galaxies in a high-mass group environment will have lower sSFRs. At low/intermediate stellar mass [$\log(M_*/M_\odot) < 10.1$], the contribution of the AGN is also small (see Fig. 2), adding further to the confidence of this conclusion.

3.2 The spatial extent of star formation in galaxy groups

We now turn to the main focus of our work, connecting the spa-

Table 3. The mean sSFR for all galaxies with $EW_{H\alpha} > 1$ Å as a function of stellar mass and environment. This includes galaxies that have central AGN/LINER/composite emission, but only star-forming spaxels are included in the estimation of the sSFR. sSFRs are given for three intervals of stellar mass and group mass (M_G), as well as ungrouped galaxies.

Stellar mass	log (sSFR/yr^{-1})		
	Ungrouped	$M_G < 10^{12.5}$	$M_G > 10^{12.5}$
$\log(M_*/M_\odot) < 9.1$	-10.10 ± 0.03	-10.04 ± 0.06	-10.49 ± 0.10
$9.1 < \log(M_*/M_\odot) < 10.1$	-10.28 ± 0.05	-10.20 ± 0.09	-10.69 ± 0.12
$\log(M_*/M_\odot) > 10.1$	-11.10 ± 0.09	-10.99 ± 0.12	-11.66 ± 0.10

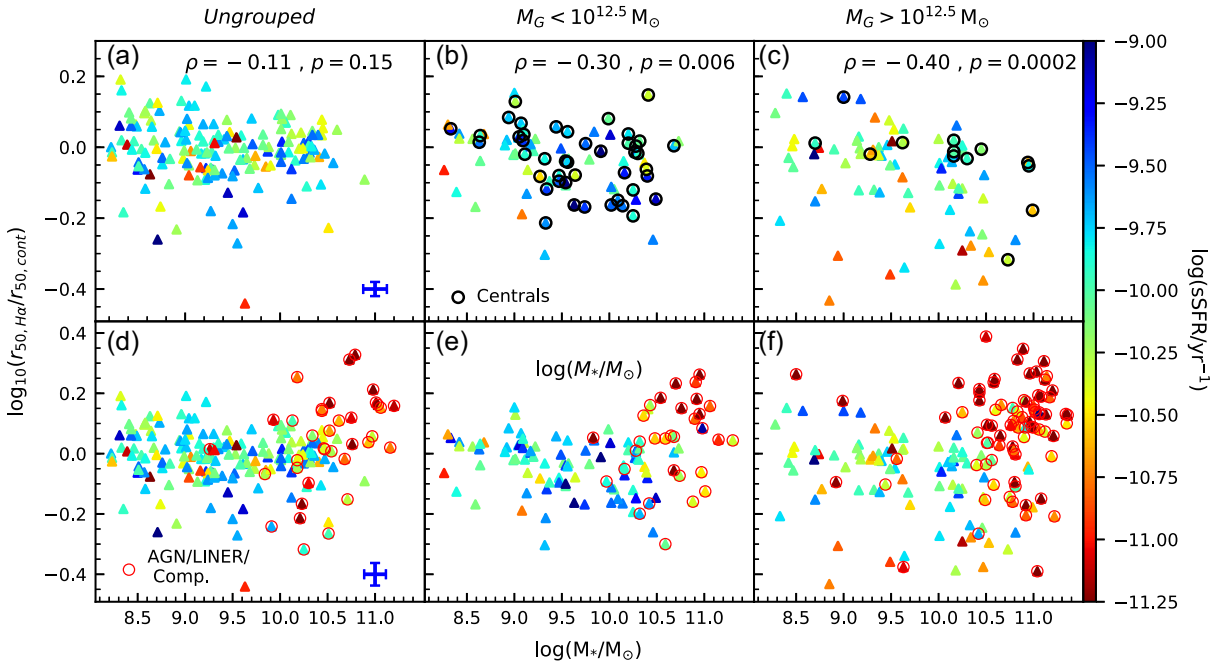

Figure 5. The scale-radius ratio as a function of stellar mass in different intervals of galaxy group halo mass, with each point coloured by the sSFR. The top row (panels *a–c*) shows only galaxies in our Final-SF sample. In the upper right of each panel, we show the Spearman rank correlation coefficient, ρ, and the associated p-value. Representative errors on each quantity are shown in blue in the lower right of panel *a*. For the ungrouped sample, there is no statistically significant correlation, but in progressively more massive groups, more massive galaxies have more centrally concentrated star formation on average. Galaxies that have been identified as the centrals in their haloes are marked with a black circle. In the lower row (panels *d–f*), we incorporate the galaxies with central AGN-like emission line ratios (Inc-Em sample). These galaxies are predominantly found at higher stellar mass, with low sSFRs, and spatially extended star formation distributions.

tial extent of star formation to a galaxy's environment. Here we will primarily focus on our star-forming sample, Final-SF, but discuss the galaxies with central AGN-like emission where appropriate (Inc-Em).

We can estimate the spatial extent of ongoing star formation using the scale-radius ratio, $r_{50,H\alpha}/r_{50,cont}$, for each galaxy in our star-forming sample (see Section 2.5.2). When this ratio is large (>1), the current star formation is more spatially extended than the distribution of the older stars. When the ratio is small (<1), the star formation is less spatially extended than the distribution of older stars.

The distribution of $r_{50,H\alpha}/r_{50,cont}$ versus stellar mass is shown in Fig. 5 (upper panels) for our three different group environments. Galaxies within our star-forming sample in the most massive groups tend to have more centrally concentrated star formation. Across the three bins of group halo mass, the relationship between the stellar mass and the spatial extent of star formation changes. For ungrouped galaxies, there is no correlation between the stellar mass and $r_{50,H\alpha}/r_{50,cont}$. The lack of a correlation is consistent with the findings of Schaefer et al. (2017), where we found no dependency of the scale-radius ratio on the stellar mass of galaxies in a smaller sample. Within groups, however, this is not the case. Galaxies in groups with $M_G < 10^{12.5}\,M_\odot$ show a slight tendency to display smaller scale-radius ratios with increasing stellar mass. In these environments, the Spearman rank correlation coefficient between $\log(M_*/M_\odot)$ and $r_{50,H\alpha}/r_{50,cont}$ is $\rho = -0.30$ with $p = 0.005$. In groups with $M_G > 10^{12.5}\,M_\odot$ the strength of the correlation between the scale-radius ratio and stellar mass is increased to $\rho = -0.40$, $p = 0.0002$.

In galaxy groups with halo masses above $10^{12.5}\,M_\odot$, galaxies with stellar masses above $\sim 10^{10}\,M_\odot$ display star formation on a smaller radial scale than for similar ungrouped galaxies. For galaxies with stellar masses less than $\sim 10^{10}\,M_\odot$, the spatial extent of star formation appears to be less dependent on the mass of the group

that the galaxy occupies. These results are summarized in Table 4, wherein we define galaxies as having 'centrally concentrated' star formation if $\log(r_{50,\mathrm{H}\alpha}/r_{50,\mathrm{cont}}) < -0.2$. Following Schaefer et al. (2017), this threshold was chosen to be 2 standard deviations below the mean for ungrouped galaxies. For galaxies with stellar masses greater than $10^{10}\,\mathrm{M}_\odot$, the fraction of galaxies that display centrally concentrated star formation rises from 4^{+4}_{-3} per cent in ungrouped galaxies to 29^{+8}_{-7} per cent in groups more massive than $10^{12.5}\,\mathrm{M}_\odot$. For galaxies below $M_* = 10^{10}\,\mathrm{M}_\odot$, there is no statistically significant change in the fraction of centrally concentrated star formers with group mass. In both ranges of galaxy stellar mass, the standard deviation from the mean of $r_{50,\mathrm{H}\alpha}/r_{50,\mathrm{cont}}$ increases in groups with halo mass greater than $10^{12.5}\,\mathrm{M}_\odot$. In low- and high-stellar-mass samples, the standard deviation in the scale-radius ratio increases by 0.033 ± 0.020 and 0.058 ± 0.015, respectively, as we move to higher group mass.

In the lower panels of Fig. 5, we include points that have previously been excluded due to central AGN-like emission (the Inc-Em sample). To determine the sSFR and $r_{50,\mathrm{H}\alpha}/r_{50,\mathrm{cont}}$ for these objects, we exclude the Hα flux from spaxels with emission-line ratios that are inconsistent with the flux being dominated by star-forming regions. Two main features are noticeable when we include these galaxies. First the AGN-like objects preferentially have extended star formation and sit above the $r_{50,\mathrm{H}\alpha}/r_{50,\mathrm{cont}} = 1$ line. This is expected as the vast majority of the AGN objects have weak LINER-like emission at their centre. This emission is likely to be caused by post-asymptotic giant branch stars, and is visible because central star formation is no longer present. Belfiore et al. (2017) related this emission to galaxies with massive bulges that are quenching from the inside out. Spindler et al. (2018) called the central LIERs (low-ionization emission regions) identified by Belfiore et al. (2017) 'centrally suppressed' galaxies. Spindler et al. (2018) find these preferentially at high stellar mass, but that their frequency of occurrence has no environmental dependence. This is consistent with our analysis of the rejection of galaxies with non-star-formation emission-line ratios in Section 2.3.1.

The majority of AGN objects shown in Fig. 5 also have low sSFRs (darker red points), below $\log(\mathrm{sSFR/yr}^{-1}) = -11$. They are likely to be mostly quenched. However, being quenched from inside out, as evidenced by their spatially extended star formation, the physical nature of the process is likely to be quite different from that of our centrally concentrated star-forming objects. The low sSFR and $r_{50,\mathrm{H}\alpha}/r_{50,\mathrm{cont}} > 1$ for the AGN is a consistent feature across all environments. This points to a mass-dependent quenching mechanism being in play for these galaxies. We find more of these galaxies in high-mass groups, but this is because high-mass galaxies are preferentially found in high-mass haloes.

A low value of $r_{50,\mathrm{H}\alpha}/r_{50,\mathrm{cont}}$ could indicate either enhanced star formation in the centre of a galaxy or reduced star formation in the outskirts (or a combination of both). Fig. 5c suggests that the centrally concentrated star-forming galaxies in high-mass groups have lower sSFRs (points with concentrated star formation are redder), so reduced star formation in their outskirts seems more likely. To further quantify this trend, we examine the relationship between the sSFRs of galaxies with the spatial extent of star formation for different group environments in Fig. 6. Here we have combined the galaxies that are ungrouped or in low-mass groups into one sample, to contrast them with the galaxies in high-mass groups. To highlight the qualitative differences in the quenching mechanisms at different stellar masses, we have divided our sample into three intervals of stellar mass. The various correlations for each stellar mass and environment interval are presented in Table 5.

For galaxies with $\mathrm{M}_* > 10^{10.1}\,\mathrm{M}_\odot$ that are either ungrouped or in group haloes less massive than $10^{12.5}\,\mathrm{M}_\odot$ (red points in Fig. 6c), there is a significant anticorrelation between the sSFR and $r_{50,\mathrm{H}\alpha}/r_{50,\mathrm{cont}}$, with Spearman's $\rho = -0.36$ and $p = 0.007$. This suggests that centrally concentrated star formation is more often associated with increased sSFR in these intermediate/low-density environments. This may be consistent with triggered star formation due to galaxy–galaxy interactions.

For galaxies with $M_* > 10^{10.1}\,\mathrm{M}_\odot$ in haloes more massive than $10^{12.5}\,\mathrm{M}_\odot$, the distribution of star formation behaves differently (black crosses in Fig. 6c). For the massive-group sample, the sSFR correlates positively with $r_{50,\mathrm{H}\alpha}/r_{50,\mathrm{cont}}$. When star formation is lowered in these galaxies, it is preferentially reduced at a larger radius, leading to more centrally concentrated star formation. There is no significant correlation between sSFR and $r_{50,\mathrm{H}\alpha}/r_{50,\mathrm{cont}}$ for lower mass galaxies in high-mass groups.

3.2.1 *The central star formation density in massive groups*

We have calculated the star formation rate surface density in a central 1 arcsec aperture in each of the star-forming galaxies in our sample. We have used these values as a further test of whether the central enhancement of star formation is able to explain the reduction in $r_{50,\mathrm{H}\alpha}/r_{50,\mathrm{cont}}$ in high-mass groups. For galaxies with stellar masses in the range $10^{10} < M_*/\mathrm{M}_\odot < 10^{10.5}$, we compare the average central star formation rate surface density for normal galaxies and for those with centrally concentrated star formation. This limited range of stellar mass was chosen to minimize the influence of the relationship between the central star formation rate surface density and stellar mass. We find that in groups with halo mass greater than $10^{12.5}\,\mathrm{M}_\odot$ the mean central star formation rate surface density is $\log(\Sigma_{\mathrm{sfr}}/\mathrm{M}_\odot\,\mathrm{yr}^{-1}\,\mathrm{kpc}^{-2}) = -1.41 \pm 0.11$ and $\log(\Sigma_{\mathrm{sfr}}/\mathrm{M}_\odot\,\mathrm{yr}^{-1}\,\mathrm{kpc}^{-2}) = -1.20 \pm 0.19$ for normal and centrally concentrated star formers, respectively. This yields a difference of 0.21 ± 0.22, which is below 1σ significance. The central star formation rate surface density in galaxies with centrally concentrated star formation is not significantly different from that of other galaxies with similar stellar mass in the same environments. The consistent central star formation surface densities also imply that the difference in concentration cannot be caused by the SFR radial profiles dropping uniformly and the outer parts of the profile dropping below our detection limit.

3.2.2 *The spatial extent of star formation and the colour–mass diagram*

The position of a galaxy on the colour–mass diagram is commonly used to diagnose its current evolutionary state. Galaxies in the blue cloud are usually star-forming or have had a recent burst of star formation, while galaxies in the red sequence are often passive and have no evidence of star formation within the last several billion years. Galaxies in between the blue cloud and red sequence are often considered to be in the process of being quenched or having their star formation rejuvenated. We display the locations of the galaxies from our Final-SF sample in this parameter space in Fig. 7 (top panels), dividing the sample into bins of group mass. The colours are dust-corrected and shifted to the rest frame of the galaxies. For our star-forming sample, we see a larger fraction of galaxies with intermediate $u - r$ colours in high-mass groups. Of these

Table 4. The scale-radius ratio of galaxies split into bins of stellar mass and group halo mass. $\langle \log (r_{50,\mathrm{H}\alpha}/r_{50,\mathrm{cont}}) \rangle$ is the mean log scale-radius ratio, σ is the standard deviation of the log scale-radius ratio, and f_{cen} is the fraction of galaxies with $\log (r_{50,\mathrm{H}\alpha}/r_{50,\mathrm{cont}}) < -0.2$.

Stellar mass range	Statistic	Ungrouped	$\log\left(\frac{M_{\mathrm{G}}}{\mathrm{M}_\odot}\right) < 12.5$	$\log\left(\frac{M_{\mathrm{G}}}{\mathrm{M}_\odot}\right) \geq 12.5$
$\log\left(\frac{M_*}{\mathrm{M}_\odot}\right) < 10$	$\langle \log (r_{50,\mathrm{H}\alpha}/r_{50,\mathrm{cont}}) \rangle$	-0.013 ± 0.009	-0.025 ± 0.012	-0.041 ± 0.018
	σ	0.093 ± 0.010	0.086 ± 0.009	0.126 ± 0.017
	f_{cen}	$0.04^{+0.02}_{-0.02}$	$0.05^{+0.03}_{-0.02}$	$0.10^{+0.05}_{-0.04}$
$\log\left(\frac{M_*}{\mathrm{M}_\odot}\right) \geq 10$	$\langle \log (r_{50,\mathrm{H}\alpha}/r_{50,\mathrm{cont}}) \rangle$	-0.005 ± 0.010	-0.063 ± 0.017	-0.124 ± 0.020
	σ	0.064 ± 0.010	0.089 ± 0.012	0.122 ± 0.011
	f_{cen}	$0.04^{+0.04}_{-0.03}$	$0.06^{+0.06}_{-0.04}$	$0.29^{+0.08}_{-0.07}$

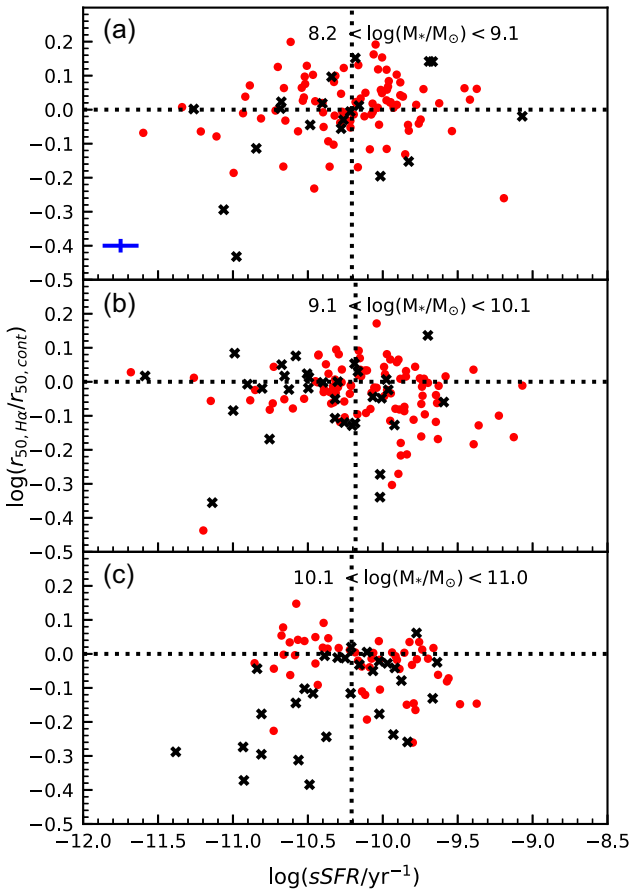

Figure 6. The scale-radius ratio as a function of the sSFR of galaxies in the stellar mass intervals shown at the top of each panel. Red points represent galaxies that either are not in groups or are in groups with halo mass less than $10^{12.5}$ $\mathrm{M}_\odot$, while black crosses are galaxies in haloes more massive than $10^{12.5}$ $\mathrm{M}_\odot$. The vertical black dotted lines represent the mean sSFR for ungrouped galaxies in each mass bin, and the horizontal dotted line represents equally extended star formation and stellar light. Significant correlations are only seen at high stellar mass (panel *c*), where we find a positive correlation between sSFR and $r_{50,\mathrm{H}\alpha}/r_{50,\mathrm{cont}}$ in high-mass groups and a negative correlation for galaxies that are in low-mass groups or are not in groups.

galaxies at intermediate colours, many have centrally concentrated H α emission. There is no evidence of such a trend in the ungrouped or low-mas- group sample. This provides further evidence that the galaxies with centrally concentrated star formation in high-mass groups are in the process of quenching.

In the lower panels of Fig. 7, we show the location of galaxies on the colour–mass plane, including those that have central AGN-like emission (marked by a red circle). The majority of them are on the red sequence, or at intermediate colours. This reiterates the point made above that most of the galaxies with central AGN-like emission are quenched or quenching. The distribution of AGN in colour–mass space appears the same for our three environmental bins, with the exception of there being a larger number of the most massive galaxies in high-mass groups.

3.3 Satellite and central galaxies

Galaxies that are environmentally quenched may experience different processes that shut down their star formation depending on where they sit within their parent group halo. A galaxy that is at the centre of a group will be less likely to experience, for example, ram pressure stripping than a galaxy that is its satellite. In galaxy groups that are dynamically relaxed, the most massive object will tend to sit at the centre of the halo, but this is not always the case (e.g. Skibba et al. 2011; Oliva-Altamirano et al. 2014). The group catalogue of Robotham et al. (2011) calculates an iterative group centre that is robust to the effects of massive galaxies in falling into groups. In this process, the galaxy that is most distant from the centre of light of the group is rejected and the centre of light is recalculated. This process is repeated until two galaxies remain, at which point the brightest of that pair is decided as the iterative centre. Robotham et al. (2011) report that in 95 per cent of cases the iterative centre is the same as the brightest group galaxy. We term galaxies in our sample that are identified as the iterative centre of their group as 'centrals' and all other group galaxies as 'satellites'. The centrals are marked by a black circle in Figs 5a–c.

As would be expected, the number of centrals we observe in groups less massive than $10^{12.5}$ $\mathrm{M}_\odot$ is large, representing a total of 48 of the 85 star-forming galaxies in this group mass bin (most of these groups have low multiplicity). These galaxies preferentially occupy the higher end of the mass distribution. We can measure the correlation between stellar mass and $r_{50,\mathrm{H}\alpha}/r_{50,cont}$ separately for the centrals and satellites, but find very little difference between the two populations. For satellites, the Spearman rank correlation coefficient is $\rho = -0.290$, with $p = 0.068$, while for centrals it is $\rho = -0.287$, with $p = 0.058$. The correlation between the spatial extent of star formation and stellar mass is similar for the satellites and centrals of groups less massive than $10^{12.5}$ $\mathrm{M}_\odot$.

Table 5. Correlation coefficients for data displayed in Fig. 6. ρ is the Spearman rank correlation coefficient between the sSFR and the scale-radius ratio in bins of stellar mass indicated in the first column and in bins of group halo mass indicated in the top row.

	Ungrouped, $M_G < 10^{12.5}$	$M_G > 10^{12.5}$	$P(\rho_1 = \rho_2)$
$8.2 < \log(M_*/M_\odot) < 9.1$	$\rho = 0.09, p = 0.42$	$\rho = 0.32, p = 0.18$	$0.9\sigma, p = 0.19$
$9.1 < \log(M_*/M_\odot) < 10.1$	$\rho = -0.20, p = 0.04$	$\rho = -0.17, p = 0.36$	$0.17\sigma, p = 0.63$
$10.1 < \log(M_*/M_\odot) < 11.0$	$\rho = -0.36, p = 0.007$	$\rho = 0.46, p = 0.009$	$3.7\sigma, p = 0.0001$

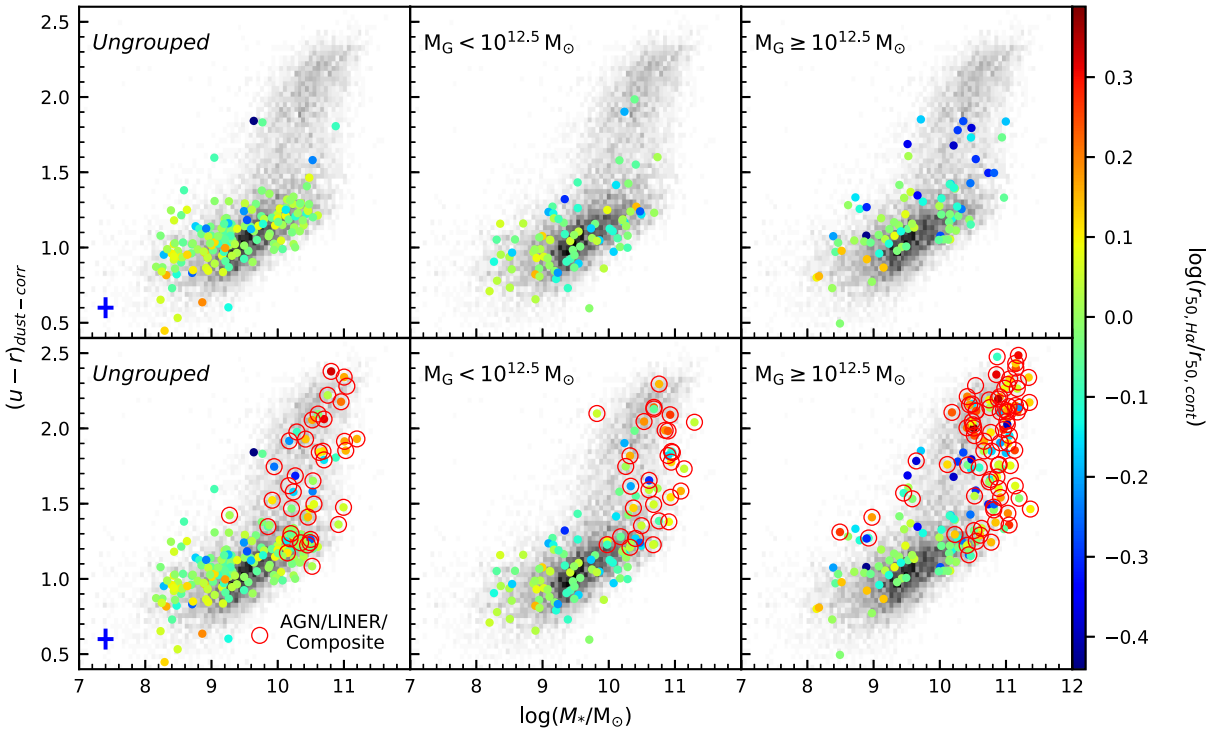

Figure 7. The position of galaxies in our star-forming sample on the $\log(M_*/M_\odot)$ versus dust-corrected, rest-frame $u - r$ colour plane. Each panel shows an interval of group halo mass, The greyscale background represents the stellar mass and intrinsic $u - r$ colour of all galaxies in the GAMA survey with $z < 0.1$, while the coloured points show the scale-radius ratio measured in SAMI galaxies. From left to right, the panels include SAMI galaxies that are ungrouped, have measured group masses less than $10^{12.5}\,M_\odot$, and have group masses above $10^{12.5}\,M_\odot$. The colour scale is the same across all three group mass bins. Galaxies moving from the blue cloud to the red sequence in massive groups tend to have centrally concentrated star formation. The upper panels shows only our star-forming sample (Final-SF), while the lower panels also includes galaxies with central AGN-like emission (red circles).

Galaxies that are the centrals of massive groups are by definition rare and, having high stellar mass, are often already passive. Of the 82 star-forming galaxies in groups more massive than $10^{12.5}\,M_\odot$, only 12 are centrals. This low number means that we are unable to make definitive statements about whether the spatial distribution of star formation in centrals differs in comparison to the star formation distribution in satellite galaxies in massive groups. In Fig. 5 we have marked central galaxies with a black circle. The correlation coefficient between $\log(M_*/M_\odot)$ and $\log(r_{50,H\alpha}/r_{50,cont})$ goes from $\rho = 0.40, p = 0.0002$ with centrals included, to $\rho = 0.41, p = 0.0005$ for satellites only.

In Fig. 6, we showed that the scale-radius ratio in galaxies with stellar masses greater than $10^{10.1}\,M_\odot$ in groups with halo mass greater than $10^{12.5}\,M_\odot$ is correlated with their sSFRs (black crosses in Fig. 6c). If we remove centrals from this sample, the strength of the correlation increases slightly, from $\rho = 0.46$ and $p = 0.009$ to $\rho = 0.53$ and $p = 0.006$, though the sample size is reduced to just 26 galaxies. In all other analysis, unless otherwise stated we do not make any distinction between satellite and central galaxies.

3.4 Galaxy–galaxy tidal interactions

A number of authors have suggested that dynamical disturbances driven by tidal interactions between galaxies in groups can cause gas to fall towards the centres of galaxies (e.g. Hernquist 1989; Moreno et al. 2015). While this may cause the enhancement of star formation on short time-scales, the consumption of gas by star formation induced by the interaction can ultimately cause the galaxy to become quenched earlier than in ungrouped galaxies. We can estimate the strength of the current tidal interaction using the perturbation parameter of Dahari (1984) and Byrd & Valtonen

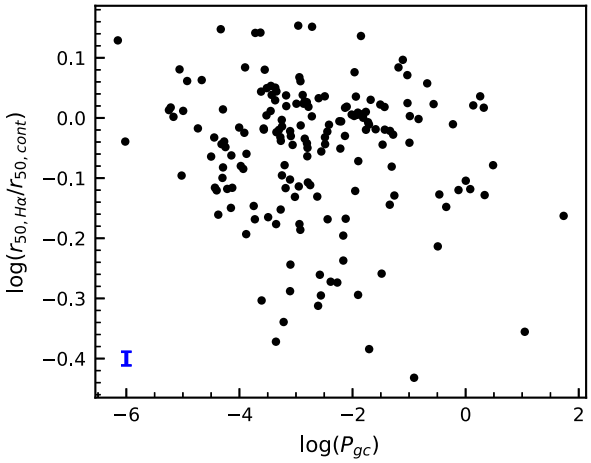

Figure 8. The scale-radius ratio as a function of the tidal perturbation parameter for galaxies in groups. With a Spearman rank correlation coefficient of $\rho = -0.06$ with $p = 0.41$, there is no evidence that the current tidal perturbation influences the radial distribution of star formation in these galaxies.

(1990)

$$P_{\rm gc} = \left(\frac{M_{\rm c}}{M_{\rm g}}\right) \times \left(\frac{r_{\rm g}}{d_{\rm gc}}\right)^3, \quad (4)$$

where $M_{\rm c}$ is the mass of the companion, $M_{\rm g}$ is the mass of the galaxy being perturbed, $r_{\rm g}$ is the optical size of the galaxy, and $d_{\rm gc}$ is the projected distance between the galaxy and its companion. Dahari (1984) and Byrd & Valtonen (1990) defined this $r_{\rm g}$ in terms of the optical sizes of galaxies as measured by hand from photographic plates, so we shall approximate this with the r-band r_{90}, the radius that contains 90 per cent of the flux, as given by the GAMA Sérsic photometric fits. Byrd & Valtonen (1990) showed that gas infall is expected when the perturbation parameter is greater than ∼0.01–0.1, depending on the halo-to-disc mass ratio. We have calculated the perturbation parameter for all possible pairs of galaxies in the GAMA Galaxy Group Catalogue and use the greatest perturbation within a group to estimate the tidal effects on a galaxy. Using this estimator of the strength of the tidal forces experienced by each galaxy in the group, we find no evidence that tidal interactions change the radial extent of star formation in galaxy groups. This is shown in Fig. 8. We must note that this does not necessarily imply that tidal interactions have no effect on the distribution of star formation in galaxies, because there could be a considerable time delay between a tidal interaction and the movement of gas to the centres of the galaxies.

3.5 Tidal interactions with the group potential

The galaxy groups in this sample can be as massive as $10^{14}\,{\rm M}_\odot$. This means that tidal perturbations in individual galaxies can be caused by their gravitational interaction with the group potential as a whole. For a galaxy with mass $M_{\rm g}$ with radius $r_{\rm g}$ located at a distance d from the centre of a group halo of mass $M_{\rm G}$, the tidal perturbation is given by

$$P_{\rm Gg} = \left(\frac{M_{\rm G}}{M_{\rm g}}\right) \times \left(\frac{r_{\rm g}}{d}\right)^3, \quad (5)$$

following Boselli & Gavazzi (2006). We calculate this value using the group mass and group-centric distances provided by the GAMA Galaxy Group Catalogue and compare it to various properties of each galaxy. In Fig. 9, we compare the group tidal perturbation to the star formation rates and distributions in our sample. We find no correlation between the group tidal perturbation and the star-forming properties of the galaxies. The lack of correlation does not necessarily rule out that tidal interactions with the group potential could alter the properties of galaxies because the metric for tidal perturbation used has large systematic uncertainties. Each galaxy's distance d from the centre of the group is subject to projection effects, in addition to the group centre being poorly defined for groups with only a few members. The use of stellar masses for the mass of each galaxy is also systematically low; the amount of dark matter in each galaxy is unknown but likely higher than the stellar mass.

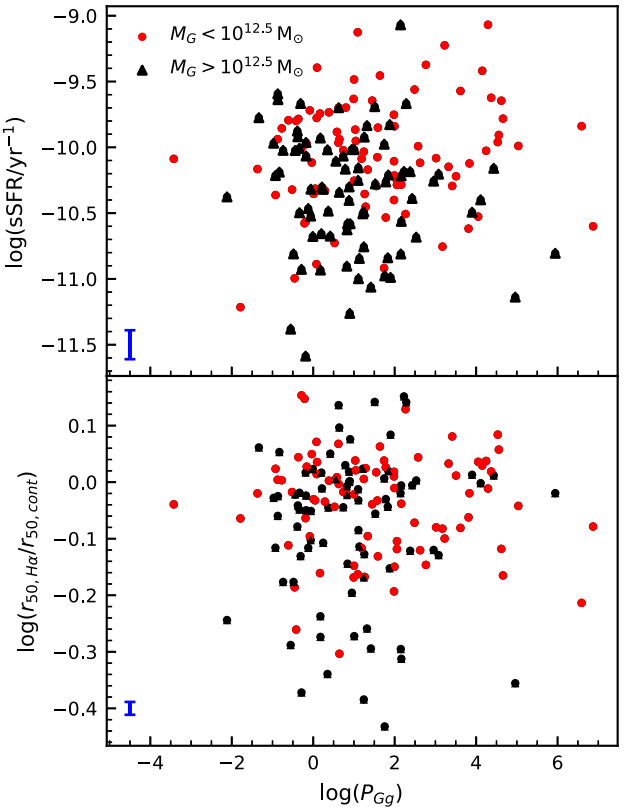

Figure 9. The star-forming properties of galaxies compared to the tidal influence of the group halo. In the upper and lower panels, we compare respectively the sSFR and scale-radius ratio to the group tidal perturbation parameter, $P_{\rm Gg}$. Black points denote galaxies in groups more massive than $10^{12.5}\,{\rm M}_\odot$ and red points indicate galaxies in lower mass groups. There is no relationship with either measurement and $P_{\rm Gg}$, though a systematic trend with the sSFR and $r_{50,{\rm H}\alpha}/r_{50,{\rm cont}}$ does exist, both quantities being lower on average in more massive groups.

3.6 Projected phase space

Some recent works have made use of projected phase-space diagrams as a means of diagnosing particular processes that may be acting on galaxies in clusters (e.g. Oman, Hudson & Behroozi 2013; Jaffé et al. 2015; Oman & Hudson 2016). In this scheme, galaxies are placed in phase space with their position and velocity measured relative to the host halo. Galaxies with velocities greater than the group velocity dispersion and within 0.5 R_{200} are likely to undergo

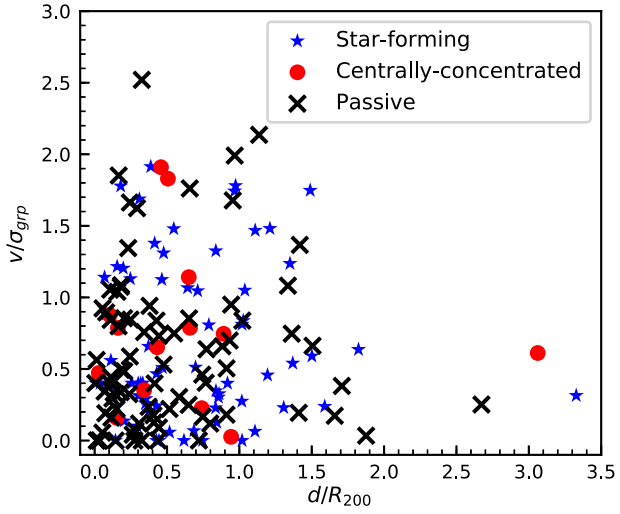

Figure 10. Projected phase-space diagram for galaxies in groups with $M_G > 10^{12.5}\,M_\odot$. The horizontal axis is the distance each galaxy is from the centre of the group, in units of R_{200}. The vertical axis is the velocity of each galaxy relative to the systemic velocity of the group normalized by the velocity dispersion of the group. Blue stars and red circles are star-forming galaxies, and black crosses are passive galaxies. Red circles represent star-forming galaxies with centrally concentrated star formation.

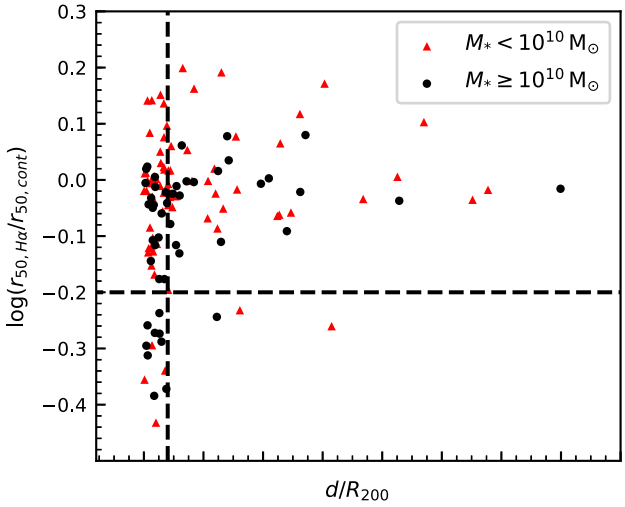

Figure 11. The scale-radius ratio for galaxies as a function of distance from the centre of the nearest group. This sample includes both galaxies that are in the GAMA Galaxy Group Catalogue and galaxies whose nearest group halo is more massive than $10^{12.5}\,M_\odot$. The horizontal dashed line is the fiducial $\log(r_{50,H\alpha}/r_{50,cont}) = -0.2$ dividing line below which we say a galaxy has centrally concentrated star formation. For $M_* > 10^{10}\,M_\odot$, galaxies with centrally concentrated star formation exist almost exclusively within R_{200}, though there is no correlation with projected group-centric distance within R_{200} in these groups.

ram pressure stripping, low-velocity galaxies far from the group centre are likely to be on their first passage through the group, and slow-moving galaxies close to the group centre are likely virialized within the group.

We calculate R_{200} for the groups in our sample using the prescription of Finn et al. (2005),

$$R_{200} = 1.73 \frac{\sigma_v}{1000\,\mathrm{km\,s^{-1}}} \frac{1}{\sqrt{\Omega_0 + \Omega_\Lambda (1+z)^3}} h_{100}^{-1}\,\mathrm{Mpc}, \quad (6)$$

where σ_v is the group velocity dispersion and z is the systemic redshift of the group.

In Fig. 10, we display all galaxies in groups more massive than $10^{12.5}\,M_\odot$ in projected phase space. Galaxies showing centrally concentrated star formation [$\log(r_{50,H\alpha}/r_{50,cont}) < -0.2$] follow the same distribution in projected phase space as other star-forming galaxies. A two-sample K–S test comparing the centrally concentrated star formers to the normal star-forming galaxies along each dimension of projected phase space showed that the distributions are not significantly different. In group-centric radius, the K–S statistic is $D = 0.21$ with p-value 0.62, and in relative velocity the K–S statistic is $D = 0.24$ with p-value 0.46. All but one of the galaxies with centrally concentrated star formation exist within R_{200} of their respective groups, and most have line-of-sight velocities relative to the group less than the group velocity dispersion.

3.7 Distribution of star formation versus group-centric radius

In Section 3.6, we saw that the distribution of centrally concentrated star-forming galaxies within R_{200} of groups more massive than $10^{12.5}\,M_\odot$ is not significantly different from that of other star-forming systems in projected phase space. We find no strong trend between $r_{50,H\alpha}/r_{50,cont}$ and group-centric radius for galaxies within groups. To highlight the difference between the galaxy populations within and outside of galaxy groups, we have matched galaxies from the ungrouped sample to the nearest group halo, within $\pm 1000\,\mathrm{km\,s^{-1}}$ from the matched group systemic velocity.

Fig. 11 shows the scale-radius ratio in galaxies in and around groups more massive than $10^{12.5}\,M_\odot$. We have split the sample into two stellar mass intervals, above and below $M_* = 10^{10}\,M_\odot$. Within these groups, closer than R_{200} to the centre of the group, there is no correlation between distance, d, and $r_{50,H\alpha}/r_{50,cont}$. For the higher stellar mass sample within R_{200}, the fraction of star-forming galaxies with centrally concentrated star formation is 35^{+9}_{-8} per cent. Outside of R_{200}, this fraction drops to 7^{+7}_{-4} per cent.[4] There are relatively few galaxies with $M_* > 10^{10}\,M_\odot$ outside of R_{200} that show the signatures of centrally confined star formation. Existing within R_{200} of a group with halo mass greater than $10^{12.5}\,M_\odot$ appears to be the primary factor in determining the outside-in quenching of star formation for galaxies with $M_* > 10^{10}\,M_\odot$. For galaxies less massive than $M_* = 10^{10}\,M_\odot$ there is no radial trend in the fraction of galaxies with concentrated star formation.

3.8 Nearest-neighbour interactions

Data from large-scale surveys have suggested that interactions between galaxies and their nearest neighbours may be able to either enhance or suppress star formation (e.g. Patton et al. 2013; Davies et al. 2015). To test this with SAMI, we use nearest-neighbour distances from the GAMA spectroscopic catalogue, including galaxies that are not necessarily in the group catalogue, but are more luminous than $M_r = -18.5$ mag. For the sample as a whole, we find no dependence of the sSFRs of galaxies on the distance to the nearest neighbour, though we note that our sample size is several orders of magnitude smaller than the large samples acquired through single-fibre spectroscopy (e.g. Ellison et al. 2008). The ratio $r_{50,H\alpha}/r_{50,cont}$

[4]These fractions differ slightly but not significantly from the fractions presented in Section 3.2. This is because those fractions included galaxies that are associated with a group but may have been farther than R_{200} from the group centre.

appears to be reduced at small separations between galaxies, but the nearest-neighbour distance is strongly correlated with group mass, obscuring any strong conclusion. To resolve this issue, we performed a partial Spearman rank correlation analysis between the group mass, nearest-neighbour distance, and $r_{50,\mathrm{H}\alpha}/r_{50,\mathrm{cont}}$ ratio for galaxies with group mass estimates. When the group mass is taken into account, the Spearman rank correlation coefficient between nearest-neighbour distance and $r_{50,\mathrm{H}\alpha}/r_{50,\mathrm{cont}}$ is found to be small and not significant ($\rho = 0.09,\ p = 0.26$).

3.8.1 The effect of close pairs

As a further test for the effect of close pairs in galaxy groups, we remove all galaxies that have a nearest neighbour of any luminosity within 50 kpc (projected distance) in the GAMA close-pair catalogue. With the close pairs removed from our sample, we repeat the analysis of Figs 5 and 6. Removing the galaxies in close pairs has the greatest impact on the high-mass-group sample, with the number of galaxies dropping from 82 to 53. In the massive groups and for galaxies more massive than $10^{10.1}\,\mathrm{M}_\odot$, the Spearman rank correlation is reduced from from $\rho = 0.46,\ p = 0.009$ to $\rho = 0.32,\ p = 0.19$. However, the difference between the correlation coefficients is not significant (the probability of them being different is 0.40). These results as well as those for other mass intervals are given in Table 6. We do not measure any significant difference when close pairs are removed from any of the samples.

Davies et al. (2015) reported different environmental effects for galaxies depending on the relative mass of their nearest neighbour. Galaxies with a more massive companion are more likely to be quenched, while those with a less massive companion are more likely to have their star formation enhanced. Our current same size is not large enough to make any meaningful comment about this distinction.

4 DISCUSSION

Taking advantage of the SAMI Galaxy Survey and the GAMA Galaxy Group Catalogue, we have examined how the spatial extent of star formation (as parametrized by $r_{50,\mathrm{H}\alpha}/r_{50,\mathrm{cont}}$) and the integrated specific star formation rate depend on environment. The rationale behind this is that the possible mechanisms at work may modify these measured quantities in different ways.

The SAMI data show that both $r_{50,\mathrm{H}\alpha}/r_{50,\mathrm{cont}}$ and the sSFR are dependent on the mass of the host halo. In particular, the signatures are different for galaxies with group masses greater than and less than $M_\mathrm{G} = 10^{12.5}\,\mathrm{M}_\odot$. We reiterate that the mean group mass of our high-mass groups is $10^{13.2}\,\mathrm{M}_\odot$ (see Fig. 1), so we are considering haloes in the group regime (not clusters). We discuss the high- and low-group-mass regimes in turn below.

4.1 Massive groups, $M_\mathrm{G} > 10^{12.5}\,\mathrm{M}_\odot$

We find that star-forming galaxies (defined as having $\mathrm{EW}_{\mathrm{H}\alpha} > 1$ Å) in massive groups have lower sSFRs than ungrouped galaxies or galaxies in low-mass groups. Similar trends have been seen by previous studies, but the reduction of the star formation rates in star-forming galaxies with the environment has been the subject of some debate in the literature. Wetzel et al. (2012) found no change in the peak sSFRs of star-forming galaxies as a function of the environment and concluded that galaxies must transition from star formation to quiescence rapidly in dense environments. This is in agreement with many others such as Balogh et al. (2004) and Peng et al. (2010). Similarly, Paccagnella et al. (2016) found no change in parameters of the star formation rate main sequence in galaxy clusters but did report a larger number of galaxies in transition between star formation and quiescence at small cluster-centric radii. This echoes the reduction in the average star formation rates of star-forming galaxies with cluster-centric radius seen by von der Linden et al. (2010).

At the heart of this discrepancy in the literature is the definition of what constitutes a 'star-forming' galaxy. Studies that employ a deeper lower limit on the star formation rate of star-forming galaxies tend to see a trend with environment. The impact of the cutoff used to separate the star-forming and passive populations of galaxies is discussed at length by Taylor et al. (2015) in the context of defining the blue cloud and red sequence on the colour–mass diagram. The same arguments apply here. Our definition of 'star-forming' is primarily constrained by the detectability of Hα emission within the galaxies in our sample. Since the SAMI spectroscopy is relatively deep, and since the integral field data are less affected by aperture effects than single-fibre spectroscopy, we are able to detect lower levels of star formation in galaxies as they make the transition towards quiescence.

Our Fig. 4 shows that the peak sSFR is shifted to lower values in our high-mass groups. In this analysis, we have used all galaxies (Full-EM sample), including those with AGN-like central spectra (only using star-forming spaxels), but because of the very small number of AGN-like objects at low/intermediate stellar mass this result is robust against issues related to bias caused by AGNs. The shift in the mean sSFR we measure is between $\Delta\log(\mathrm{sSFR/yr}^{-1}) = -0.38 \pm 0.10$ and -0.64 ± 0.14 (from low to high stellar mass) and a similar result is found if we estimate the median. This is a significant difference in all three galaxy stellar mass intervals. The mean over all galaxy stellar masses is -0.45 ± 0.07, and there is no significant change in this value with stellar mass. Rasmussen et al. (2012) use UV photometry from GALEX to find a similar decrease in the sSFR of low-mass star-forming galaxies in groups. However, they find no suppression for high-stellar-mass galaxies ($M_* > 10^{10}\,\mathrm{M}_\odot$). This difference may be caused by the more restrictive dynamic range used to define star-forming galaxies [$\log(\mathrm{sSFR/}yr^{-1}) > -10.5$] in the work of Rasmussen et al. (2012). In contrast, Wetzel et al. (2012) (fitting a skewed Gaussian to the star-forming and passive populations) find differences of $\Delta\log(\mathrm{sSFR/yr}^{-1}) = -0.2$ or less (their Fig. 1) and argue there is no significant difference between centrals and satellites that are star-forming, whatever the mass of the halo. The potential causes of the difference with Wetzel et al. (2012) include aperture effects and their use of D_n4000 as a star formation indicator when Hα is weak or obscured by an AGN, as this provides an upper limit to the true sSFR.

Using a sample of purely star-forming galaxies (Final-SF), we find that galaxies in groups with $M_\mathrm{G} > 10^{12.5}\,\mathrm{M}_\odot$, with stellar masses greater than $\sim 10^{10}\,\mathrm{M}_\odot$, have more centrally concentrated star formation than the same-mass galaxies in lower mass haloes. This trend is not observed for galaxies at lower stellar masses. Such a result is in agreement with our previous analysis measuring the radial Hα gradients of SAMI galaxies as a function of the fifth-nearest-neighbour density (Schaefer et al. 2017). The process that is environmentally quenching these galaxies is acting from outside in.

While the observations above do not tell us directly what the process of quenching is, the measurements of sSFR and concentration have at least two implications for our understanding of the quenching process:

Table 6. The strengths of the correlations between the sSFR and scale-radius ratio in galaxies in different bins of stellar mass and group halo mass. Also shown are the strengths of the correlations when close pairs (< 50 kpc separation) are removed. We have provided the significance of the difference in correlations, σ, and the probability P that they are the same. In our sample, galaxies in close pairs do not significantly affect our results.

		Ungrouped, $M_{\rm G} < 10^{12.5}$	$P(\rho_{\rm pairs} = \rho_{\rm no\,pairs})$	$M_{\rm G} > 10^{12.5}$	$P(\rho_{\rm pairs} = \rho_{\rm no\,pairs})$
$8.2 < \log(M_*/{\rm M}_\odot) < 9.1$	pairs	$\rho = 0.09, p = 0.42$	0.28σ	$\rho = 0.32, p = 0.18$	-0.05σ
	no pairs	$\rho = 0.13, p = 0.26$	$P = 0.76$	$\rho = 0.30, p = 0.26$	$P = 0.96$
$9.1 < \log(M_*/{\rm M}_\odot) < 10.1$	pairs	$\rho = -0.20, p = 0.04$	$6 \times 10^{-4}\sigma$	$\rho = -0.17, p = 0.36$	0.49σ
	no pairs	$\rho = -0.20, p = 0.06$	$P = 1.0$	$\rho = -0.02, p = 0.94$	$P = 0.62$
$10.1 < \log(M_*/{\rm M}_\odot) < 11.0$	pairs	$\rho = -0.36, p = 0.007$	0.04σ	$\rho = 0.46, p = 0.009$	-0.53σ
	no pairs	$\rho = -0.35, p = 0.016$	$P = 0.96$	$\rho = 0.32, p = 0.19$	$P = 0.60$

(i) the lower sSFR of star-forming galaxies in high-mass groups means that the environmental quenching of star formation within these groups cannot be faster than the time-scale taken from the birth to death of OB stars. It is these OB stars that excite H α emission in H II regions. If quenching occured on a time-scale shorter than this, we would not see the lowering of the mean sSFR in the most massive groups. Instead we would only see an increase in the quenched fraction of galaxies.

(ii) Either low-mass galaxies and high-mass galaxies quench by a different mechanism or a single mechanism causes the effects that we observe, but this mechanism affects the distribution of star formation in a way that depends on the stellar mass. For example, if the time-scale for the outside-in quenching of low-mass galaxies is substantially shorter than for high-mass galaxies, we would observe fewer centrally concentrated star-forming galaxies at low stellar mass.

For our pure star-forming sample (Final-SF), we have also quantified the change in the scatter of $r_{50,{\rm H}\alpha}/r_{50,{\rm cont}}$ with environment (see Table 4). There is an increased scatter at high group mass and for high-mass galaxies this increased scatter is preferentially to lower $r_{50,{\rm H}\alpha}/r_{50,{\rm cont}}$. That is, while some galaxies in more massive groups have radial star formation distributions similar to those in ungrouped galaxies, a significant fraction have more centrally concentrated star formation [$\log(r_{50,{\rm H}\alpha}/r_{50,{\rm cont}}) < -0.2$], and very few have more extended star formation. In particular, in our final star-forming sample, 29^{+8}_{-7} per cent of galaxies more massive than $M_* = 10^{10}\,{\rm M}_\odot$ in the massive group sample have $\log(r_{50,{\rm H}\alpha}/r_{50,{\rm cont}}) < -0.2$, compared to 4^{+2}_{-2} per cent in ungrouped galaxies. The increase in the scatter in $r_{50,{\rm H}\alpha}/r_{50,{\rm cont}}$ suggests some inefficiency in the outside-in quenching process. It is not clear whether this process acts on all galaxies that fall into these groups, or whether the inclination of the galaxy disc to the direction of passage through the IGM influences the change in the star formation distribution, as has been predicted by simulations of ram pressure stripping in galaxy groups and clusters (e.g. Bekki 2014).

Fig. 7 suggests that the star-forming galaxies in our sample occupy different distributions in the colour–mass diagram depending on the mass of the parent halo. Above $M_{\rm G} = 10^{12.5}\,{\rm M}_\odot$, a larger fraction of galaxies are in transition between the blue cloud and the red sequence, particularly for systems with $M_* > 10^{10}\,{\rm M}_\odot$. This has been reported by a number of studies using unresolved data in the past (e.g. Balogh et al. 2004; Hogg et al. 2004; Bassett et al. 2013). Schawinski et al. (2014) showed that late-type galaxies in haloes more massive than $10^{12}\,{\rm M}_\odot$ are much more likely to lie off the blue cloud in the colour–mass diagram. Their modelling showed that the time-scale for a late-type galaxy to make the transition from the blue cloud to the red sequence is of order several Gyr but that this can be accelerated by various environmental processes. Our results indicate that a fraction of this transitioning population of galaxies can be explained by an outside-in quenching mechanism that is consistent with gas stripping.

Within groups with halo mass greater than $10^{12.5}\,{\rm M}_\odot$, we find no significant projected phase-space differences between galaxies with centrally concentrated star formation and passive or normally star-forming galaxies. If outside-in quenching of star formation started in these galaxies soon after their infall into these massive groups, we would expect a greater separation of these two types of galaxies in projected phase space. However, if the efficiency of the mechanism that causes this change in the star formation morphology is poor, or its onset is delayed, the distribution of galaxies with centrally concentrated star formation is easily explained. Being within $\sim R_{200}$ is important to the outside-in quenching to take place, as the fraction of centrally concentrated star-forming galaxies is significantly lower outside of this radius.

Jaffé et al. (2015) detected the 21 cm neutral hydrogen emission line in galaxies outside the virialized region of galaxy clusters, but did not detect this line for galaxies inside the virialized region, where they have presumably resided in the clusters for several cluster dynamical times. Given the difference in halo mass between the groups in our sample and the cluster studied by Jaffé et al. (2015), it is difficult to draw direct comparisons, but it seems probable that many of the galaxies with centrally concentrated star formation are not on their first passage into their host groups. This is consistent with Brown et al. (2017) who find a deficit of neutral gas, even in relatively low-mass groups ($10^{12} - 10^{13.5}\,{\rm M}_\odot$).

Comparing the distribution of these galaxies to the simulations of projected phase space performed by Oman et al. (2013), we can conclude that the majority of centrally concentrated star-forming galaxies have been in their groups for perhaps over three Gyr (see Oman et al. 2013, their fig. 4). We interpret the distribution of these galaxies in projected phase space as a sign that the quenching of star formation by this outside-in mechanism is not instantaneous and persists over several group-crossing times.

Peng et al. (2015) used stellar metallicities to infer that starvation is expected to be the primary quenching route. The single-fibre SDSS data used by Peng et al. (2015) only sample the inner parts of galaxies, meaning that a possible picture in high-mass groups is for galaxies to suffer partial outside-in ram pressure stripping. The central parts of the galaxies, which have not been stripped, then slowly quench via starvation.

4.2 Low-mass groups, $M_G < 10^{12.5}\,M_\odot$

In contrast to the environmental suppression of star formation in galaxies in the high-mass-group sample, we find that for galaxies in low-mass groups (i.e. with halo mass $M_G < 10^{12.5}\,M_\odot$), there is little evidence for environmental quenching in galaxies. We find that in these systems there is some evidence that centrally concentrated star formation is related to an *increase* in the sSFR for galaxies with stellar mass $>10^{10.1}\,M_\odot$.

A similar effect was noted by Davies et al. (2015) when studying the star formation rates of pairs of galaxies in the GAMA catalogue. They showed that the more massive galaxies in pairs have centrally enhanced star formation, while the lower mass companion had its star formation suppressed. The enhancement of star formation in close pairs was reported by Ellison et al. (2008). This picture is broadly consistent with the simulations presented by Moreno et al. (2015), who showed that a close encounter between two galaxies will trigger the enhancement of star formation in a galaxy's centre. It is unclear whether we are observing the same trend as Davies et al. (2015) and Ellison et al. (2008), as they observed enhancement only in late-stage mergers, and we have a substantially smaller sample and fewer galaxy pairs at small separations. The trends that we have reported here apply to galaxies separated from their nearest neighbour by more than 30 kpc.

Another possible explanation of our results comes from interpreting our data in the context of the discussion presented by Janowiecki et al. (2017). In this work, the authors observe that in galaxies in groups with only two members, the central tends to have higher a H I content than galaxies in isolation at the same stellar mass. These H i-rich systems were observed to have higher sSFRs as well. From these observations, the authors suggest that gas-rich minor mergers or direct feeding of gas from the IGM may be more common in such environments. The acquisition of H I gas mass measurements for our sample would allow us to comment further on this point.

4.3 Other metrics for interaction

4.3.1 Tidal interactions

We do not find any significant correlation between the estimated strength of the tidal interaction between galaxies and their star-forming properties. The apparent strength of the tidal force acting on a galaxy, calculated from equation (4), influences neither the total measured specific star formation nor the scale radius of star formation relative to the scale radius of the stellar light. Superficially this might seem to contradict results from simulations (Hernquist 1989; Moreno et al. 2015) that suggest a central burst of star formation can occur in a galaxy after a close encounter with a companion if gas is present. However, our measurement of P_{gc} is susceptible to systematic uncertainties imposed by projection effects when estimating the separation between two galaxies. The effect of projection will be to increase our estimate of the tidal interaction strength, and as such each measurement is at best an upper limit. A further shortcoming of this technique results from the fact that there is a delay between the time of closest approach for two systems and the time at which nuclear star formation will be triggered and is able to be measured. This delay, and the inability to distinguish between systems infalling towards an interaction and those that are moving away after an interaction, makes identifying the signatures of tidal interactions difficult with this technique. Therefore, we cannot rule out the possibility that tidal interactions cause quenching in high-mass galaxy groups or enhancement in low-mass groups.

4.3.2 Close-pair interactions

Close-pair interactions have been reported to drive much of the environmental evolution of galaxies, including enhancing and suppressing their star formation (López-Sánchez & Esteban 2008, 2009; Robotham et al. 2014; Davies et al. 2015). We have found no statistically significant link between the nearest-neighbour distance and either $r_{50,H\alpha}/r_{50,cont}$ or the sSFRs of galaxies in our sample. However, we note that our sample contains low numbers of galaxies at separations small enough to adequately test the predictions of these previous studies. A more comprehensive study of the distribution of star formation in close pairs of galaxies will be possible once the full SAMI survey has been completed and a larger sample of close pairs can be constructed.

4.4 Comparison to other work

Our results have built on the work presented in Schaefer et al. (2017), and we find general agreement with the trends presented therein. While our previous work compared the spatial extent of star formation to the fifth-nearest-neighbour surface density environment measure, the use of galaxy group properties has provided a framework for a more physical understanding of the processes at play. In contrast to Schaefer et al. (2017), we find an anticorrelation between the scale-radius ratio and the stellar mass of the galaxies, but only find this in more massive group haloes. The quenching of galaxies with stellar mass greater than $10^{10}\,M_\odot$ from the outside-in in dense environments is consistent with our previous findings, with the lack of this signature at lower stellar masses made more significant by our expanded sample.

These results from SAMI echo the findings from the H α narrow-band imaging presented in Kulkarni (2015). Kulkarni observed that galaxies with small scale-radius ratios lie below the star formation main sequence. The centrally confined distribution of star formation in these galaxies, along with an observed flattening in the stellar light profiles in the outskirts of the galaxies, led them to conclude that a combination of ram pressure stripping and gravitational interactions is the primary mechanism influencing group galaxies today. While with SAMI we are unable to investigate the outer stellar discs of our sample, we do find agreement in the star formation morphologies. A future study that combines the radial coverage of narrow-band imaging with the spectroscopic advantages of integral field surveys will yield important clues as to the relative impact of these two processes on shaping the galaxy populations of today.

The radial distribution of star formation was also investigated by Spindler et al. (2018), using data from the MaNGA survey. These authors found a very weak correlation between the star formation rate gradients in galaxies and the local environment density in comparison to Schaefer et al. (2017). This discrepancy can be reconciled by understanding the difference in the sample selection between the two studies. While Schaefer et al. (2017) eliminated galaxies with AGN-like central spectra (in the same way as the Final-SF sample in this work), Spindler et al. (2018) did not. The consequence of these choices is illustrated in Fig. 5. Comparing panels *c* and *f* shows that the inclusion of what Spindler et al. (2018) term 'centrally suppressed' star-forming galaxies has the effect of washing out the more subtle signatures of environment quenching.

Bekki (2014) produced hydrodynamical simulations of the ram pressure stripping of gas from galaxies in groups and clusters. With these simulations, they showed that the scale size of the star-forming discs of galaxies under ram pressure stripping can be reduced by a factor of 2 or more, depending on the halo mass of the group. The simulated galaxies under the influence of ram pressure stripping could have their star formation either enhanced or suppressed. For high-mass satellite galaxies ($M_* > 10^{10}\,\mathrm{M}_\odot$) in our massive-group sample, a reduction in the scale size of the star-forming disc is generally accompanied by a reduction in the total specific sSFR. The galaxies for which we do see a reduced scale-radius ratio accompanied by an enhancement of the integrated star formation rate are the centrals of low-mass-group haloes and are unlikely to be undergoing ram pressure stripping and are perhaps more likely to have undergone recent minor mergers or experienced fuelling from extragalactic gas (Janowiecki et al. 2017).

Analytical modelling by Hester (2006) showed qualitatively similar results to Bekki (2014). In their work, they showed that the extent to which a galaxy is stripped of its gas by ram pressure depends on the mass distribution within a galaxy, and its trajectory through a cluster or group of a given mass. They showed that for galaxies moving through a group, it is possible for quenching to occur in just the outer parts of the disc. This provides a natural way of having ram pressure stripping quench star formation slowly or partially in the range of halo masses that we study here.

5 CONCLUSION

We have used data from the SAMI Galaxy Survey to study the processes that suppress star formation in groups identified in the GAMA Galaxy Group Catalogue. The GAMA data provided several different metrics by which to quantify the environments of the galaxies in our sample.

Our analysis shows a suppression of star formation in star-forming galaxies within high-mass groups ($M_\mathrm{G} > 10^{12.5}\,\mathrm{M}_\odot$) at all galaxy stellar masses. This is hard to reconcile with models of instantaneous quenching.

We find that the concentration of star formation is correlated with galaxy stellar mass in high-mass groups. Galaxies with stellar masses above approximately $10^{10}\,\mathrm{M}_\odot$ in high-mass groups are more likely to have concentrated star formation. The fraction with concentrated star formation in the Final-SF sample is 29^{+8}_{-7} per cent, compared to 4^{+3}_{-4} per cent for similar galaxies that are not in groups. This central confinement of the star formation is also associated with a reduction in the total star formation rate, with no strong evidence for central enhancement of star formation. The concentration of star formation in these galaxies suggests a process such as ram pressure stripping. However, the location of these galaxies on the colour–mass plane, together with no separation between them and other galaxies in projected phase space, suggests a relatively long time-scale for this to occur. This mechanism appears only to act within R_{200} of the centres of these massive groups.

In the same massive groups, galaxies with stellar masses less than $10^{10}\,\mathrm{M}_\odot$ show less evidence of centrally concentrated star formation. This may infer a faster or more uniform quenching process but one that still results in an overall reduction in the specific sSFR of star-forming galaxies.

In lower mass groups ($M_\mathrm{G} < 10^{12.5}\,\mathrm{M}_\odot$), we find no evidence of quenching. Instead we find some evidence that centrally concentrated star formation is correlated with an increase in the overall sSFR. This may be related to triggered star formation.

ACKNOWLEDGEMENTS

We gratefully acknowledge the useful feedback and input from the anonymous referee, which improved the quality of this work.

The SAMI Galaxy Survey is based on observations made at the Anglo-Australian Telescope. The Sydney-AAO Multi-object Integral field spectrograph (SAMI) was developed jointly by the University of Sydney and the Australian Astronomical Observatory. The SAMI input catalogue is based on data taken from the Sloan Digital Sky Survey, the Galaxy And Mass Assembly (GAMA) Survey, and the VST ATLAS Survey. The SAMI Galaxy Survey is supported by the Australian Research Council Centre of Excellence for All Sky Astrophysics in 3 Dimensions (ASTRO 3D), through project number CE170100013, the Australian Research Council Centre of Excellence for All-sky Astrophysics (CAASTRO), through project number CE110001020, and other participating institutions. The SAMI Galaxy Survey website is http://sami-survey.org/.

GAMA is a joint European–Australasian project based around a spectroscopic campaign using the Anglo-Australian Telescope. The GAMA website is http://www.gama-survey.org/.

M.S.O. acknowledges the funding support from the Australian Research Council (ARC) through a Future Fellowship (FT140100255). J.T.A. acknowledges the award of a Science and Industry Endowment Fund (SIEF) John Stocker Fellowship. J.v.d.S. is funded under Bland-Hawthorn's ARC Laureate Fellowship (FL140100278). S.B. acknowledges the funding support from the Australian Research Council through a Future Fellowship (FT140101166). S.K.Y. acknowledges support from the Korean National Research Foundation (2017R1A2A1A05001116) and by the Yonsei University Future Leading Research Initiative (2015-22-0064). This study was performed under the umbrella of the joint collaboration between Yonsei University Observatory and the Korean Astronomy and Space Science Institute. C.F. gratefully acknowledges funding provided by the Australian Research Council's Discovery Projects (grants DP150104329 and DP170100603). Support for A.M.M. is provided by National Aeronautics and Space Adminsitration (NASA) through Hubble Fellowship grant #HST-HF2-51377 awarded by the Space Telescope Science Institute, which is operated by the Association of Universities for Research in Astronomy, Inc., for NASA, under contract NAS5-26555.

This research made use of ASTROPY, a community-developed core PYTHON package for Astronomy (Astropy Collaboration 2013). We also used the NUMPY and SCIPY scientific PYTHON libraries.

REFERENCES

Abazajian K. N. et al., 2009, ApJS, 182, 543
Allen J. T. et al., 2015, MNRAS, 446, 1567
Alpaslan M. et al., 2015, MNRAS, 451, 3249
Astropy Collaboration, 2013, A&A, 558, A33
Bahé Y. M., McCarthy I. G., Balogh M. L., Font A. S., 2013, MNRAS, 430, 3017
Baldwin J. A., Phillips M. M., Terlevich R., 1981, PASP, 93, 5
Balogh M. L., Baldry I. K., Nichol R., Miller C., Bower R., Glazebrook K., 2004, ApJ, 615, L101
Bassett R. et al., 2013, ApJ, 770, 58
Bekki K., 2014, MNRAS, 438, 444
Belfiore F. et al., 2017, MNRAS, 466, 2570
Bianconi M., Smith G. P., Haines C. P., McGee S. L., Finoguenov A., Egami E., 2018, MNRAS, 473, L79
Bland-Hawthorn J. et al., 2011, OExpr, 19, 2649
Boselli A. et al., 2014, A&A, 570, A69
Boselli A. et al., 2016, A&A, 596, A11
Boselli A., Gavazzi G., 2006, PASP, 118, 517

Brough S. et al., 2013, MNRAS, 435, 2903
Brown T. et al., 2017, MNRAS, 466, 1275
Bryant J. J., Bland-Hawthorn J., Fogarty L. M. R., Lawrence J. S., Croom S. M., 2014, MNRAS, 438, 869
Bryant J. J. et al., 2015, MNRAS, 447, 2857
Byrd G., Valtonen M., 1990, ApJ, 350, 89
Calzetti D., 2001, PASP, 113, 1449
Cappellari M., Emsellem E., 2004, PASP, 116, 138
Cardelli J. A., Clayton G. C., Mathis J. S., 1989, ApJ, 345, 245
Cayatte v., Van Gorkom J. H., Balkowski C., Kotanyi C, 1990, AJ, 100, 604
Chabrier G., 2003, PASP, 115, 763
Cibinel A. et al., 2013, ApJ, 777, 116
Colless M. et al., 2001, MNRAS, 328, 1039
Cortese L. et al., 2010, A&A, 518, L49
Cortese L. et al., 2012, A&A, 544, A101
Cox D. R., 1958, J. R. Stat. Soc. Ser. B, 20, 215
Croom S., Saunders W., Heald R., 2004, AAONw, 106, 12
Croom S. M. et al., 2012, MNRAS, 421, 872
Dahari O., 1984, AJ, 89, 966
Davies L. J. M. et al., 2015, MNRAS, 452, 616
Davies L. J. M. et al., 2016a, MNRAS, 455, 4013
Davies R. L. et al., 2016, MNRAS, 462, 1616
Driver S. P. et al., 2011, MNRAS, 413, 971
Eigenthaler P., Ploeckinger S., Verdugo M., Ziegler B., 2015, MNRAS, 451, 2793
Eke V. R. et al., 2004, MNRAS, 348, 866
Ellison S. L., Patton D. R., Simard L., McConnachie A. W., 2008, AJ, 135, 1877
Finn R. A. et al., 2005, ApJ, 630, 206
Fujita Y., Goto T., 2004, PASJ, 56, 621
Gavazzi G., Fumagalli M., Fossati M., Galardo V., Grossetti F., Boselli A, Giovanelli R., Haynes M. P., 2013, A&A, 553, A89
Geha M., Blanton M. R., Yan R., Tinker J. L., 2012, ApJ, 757, 85
Gunn J. E., Gott J. R., III, 1972, ApJ, 176, 1
Hernquist L., 1989, Nature, 340, 687
Hester J. A., 2006, ApJ, 647, 910
Hogg D. W. et al., 2004, ApJ, 601, L29
Ho I.-T. et al., 2016, Ap&SS, 361, 280
Hopkins A. M. et al., 2013, MNRAS, 430, 2047
Jaffé Y. L., Smith R., Candlish G. N., Poggianti B. M., Sheen Y.-K., Verheijen M. A. W., 2015, MNRAS, 448, 1715
Janowiecki S., Catinella B., Cortese L., Saintonge A., Brown T., Wang J., 2017, MNRAS, 466, 4795
Kauffmann G. et al., 2003a, MNRAS, 341, 54
Kauffmann G. et al., 2003b, MNRAS, 346, 1055
Kelvin L. S. et al., 2012, MNRAS, 421, 1007
Kennicutt R. C., Jr, 1998, ApJ, 498, 541
Kewley L. J., Dopita M. A., Sutherland R. S., Heisler C. A., Trevena J., 2001, ApJ, 556, 121
Kewley L. J., Geller M. J., Jansen R. A., Dopita M. A., 2002, AJ, 124, 3135
Koopmann R. A., Kenney J. D. P., 2004a, ApJ, 613, 851
Koopmann R. A., Kenney J. D. P., 2004b, ApJ, 613, 866
Koopmann R. A., Haynes M. P., Catinella B., 2006, AJ, 131, 716
Kulkarni S., 2015, PhD thesis, Ludwig-Maximilians-Universität
Larson R. B., Tinsley B. M., Caldwell C. N., 1980, ApJ, 237, 692
Lewis I. et al., 2002, MNRAS, 334, 673
Liske J. et al., 2015, MNRAS, 452, 2087
López-Sánchez Á. R., Esteban C., 2008, A&A, 491, 131
López-Sánchez A. R., Esteban C., 2009, A&A, 508, 615
Markwardt C. B., 2009, ASPC, 411, 251
Mok A, Wilson C. D., Knapen J. H., Sánchez-Gallego J. R., Brinks E., Rosolowsky E., 2017, MNRAS, 467, 4282
Moreno J., Torrey P., Ellison S. L., Patton D. R., Bluck A. F. L., Bansal G., Hernquist L., 2015, MNRAS, 448, 1107
Oliva-Altamirano P. et al., 2014, MNRAS, 440, 762
Oman K. A., Hudson M. J., 2016, MNRAS, 463, 3083
Oman K. A., Hudson M. J., Behroozi P. S., 2013, MNRAS, 431, 2307
Owers M. S. et al., 2017, MNRAS, 468, 1824
Paccagnella A. et al., 2016, ApJ, 816, L25
Patton D. R., Torrey P., Ellison S. L., Mendel J. T., Scudder J. M., 2013, MNRAS, 433, L59
Peng Y., Maiolino R., Cochrane R., 2015, Nature, 521, 192
Peng Y.-j. et al., 2010, ApJ, 721, 193
Peng Y.-j., Lilly S. J., Renzini A., Carollo M., 2012, ApJ, 757, 4
Rasmussen J., Mulchaey J. S., Bai L., Ponman T. J., Raychaudhury S., Dariush A., 2012, ApJ, 757, 122
Robotham A. S. G. et al., 2011, MNRAS, 416, 2640
Robotham A. S. G. et al., 2014, MNRAS, 444, 3986
Rudnick G. et al., 2017, ApJ, 850, 181
Schaefer A. L. et al., 2017, MNRAS, 464, 121
Schawinski K. et al., 2014, MNRAS, 440, 889
Sharp R. et al., 2015, MNRAS, 446, 1551
Skibba R. A., van den Bosch F. C., Yang X., More S., Mo H., Fontanot F., 2011, MNRAS, 410, 417
Spindler A. et al., 2018, MNRAS, 476, 580
Springel V. et al., 2005, Nature, 435, 629
Taylor E. N. et al., 2011, MNRAS, 418, 1587
Taylor E. N. et al., 2015, MNRAS, 446, 2144
Tonry J. L., Blakeslee J. P., Ajhar E. A., Dressler A., 2000, ApJ, 530, 625
van de Sande J. et al., 2017, ApJ, 835, 104
Vazdekis A., Sánchez-Blázquez P., Falcón-Barroso J., Cenarro A. J., Beasley M. A., Cardiel N., Gorgas J., Peletier R. F., 2010, MNRAS, 404, 1639
Viola M. et al., 2015, MNRAS, 452, 3529
von der Linden A., Wild V., Kauffmann G., White S. D. M., Weinmann S., 2010, MNRAS, 404, 1231
Walker A. R., Duncan D. B., 1967, Biometrika, 54, 167
Wetzel S. H., Tinker J. L., Conroy C., 2012, MNRAS, 424, 232
Wetzel A. R., Tinker J. L., Conroy C., van den Bosch, 2013, MNRAS, 432, 336
Wheeler C., Phillips J. I., Cooper M. C., Boylan-Kolchin M., Bullock J. S., 2014, MNRAS, 442, 1396
Wijesinghe D. B. et al., 2011, MNRAS, 410, 2291
Wijesinghe D. B. et al., 2012, MNRAS, 423, 3679
Yang X., Mo H. J., van den Bosch F. C., Pasquali A., Li C., Barden M., 2007, ApJ, 671, 153
York D. G. et al., 2000, AJ, 120, 1579
Zabludoff A. I., Zaritsky D., Lin H., Tucker D., Hashimoto Y., Shectman S. A., Oemler A., Kirshner R. P., 1996, ApJ, 466, 104

This paper has been typeset from a TEX/LATEX file prepared by the author.